

University of Nebraska - Lincoln

DigitalCommons@University of Nebraska - Lincoln

Dissertations & Theses in Earth and Atmospheric
Sciences

Earth and Atmospheric Sciences, Department of

12-2016

Hail Variability in Supercell Storms and Response to Environmental Variables

Lena V. Heuscher

University of Nebraska-Lincoln, lena.heuscher@huskers.unl.edu

Follow this and additional works at: <http://digitalcommons.unl.edu/geoscidiss>

Heuscher, Lena V., "Hail Variability in Supercell Storms and Response to Environmental Variables" (2016). *Dissertations & Theses in Earth and Atmospheric Sciences*. 87.

<http://digitalcommons.unl.edu/geoscidiss/87>

This Article is brought to you for free and open access by the Earth and Atmospheric Sciences, Department of at DigitalCommons@University of Nebraska - Lincoln. It has been accepted for inclusion in Dissertations & Theses in Earth and Atmospheric Sciences by an authorized administrator of DigitalCommons@University of Nebraska - Lincoln.

HAIL VARIABILITY IN SUPERCELL STORMS AND
RESPONSE TO ENVIRONMENTAL VARIABLES

By

Lena V. Heuscher

A THESIS

Presented to the Faculty of

The Graduate College at the University of Nebraska

In Partial Fulfillment of Requirements

For the Degree of Master of Science

Major: Earth and Atmospheric Sciences

Under the Supervision of Professor Matthew Van Den Broeke

Lincoln, Nebraska

December, 2016

HAIL VARIABILITY IN SUPERCELL STORMS AND RESPONSE TO ENVIRONMENTAL VARIABLES

Lena V. Heuscher, M.S.

University of Nebraska, 2016

Advisor: Matthew Van Den Broeke

Severe weather events in the United States including tornadoes, hail, and wind are often produced by supercell thunderstorms. These storms are characterized by complex hydrometeor distributions which can be influenced by environmental distributions of wind and moisture. Since the Weather Surveillance Radar-1988 Doppler (WSR-88D) network was fully upgraded to dual-polarimetric capabilities in 2013, dominant hydrometeor species such as hail have been inferable using fuzzy logic. In this study, time series of areal extent of the inferred hail signature at base scan level have been estimated for 145 supercell storms, including both tornadic and non-tornadic cases, across a variety of environments from February 2012-December 2014. Proximity soundings were gathered for environments representative of the supercells (e.g., on the same side of mesoscale boundaries, in a region representative of storm-relative inflow) using archived Rapid Update Cycle (RUC) and Rapid Refresh (RAP) model output from the National Operational Model Archive and Distribution System (NOMADS). Model sounding points were within ~80 km and the midpoint of the analysis period in order to spatiotemporally represent environments during the period in which storms were analyzed. Previous modeling and observational studies have shown that thermodynamic,

moisture, and shear parameters influence the mean areal extent of hail at the base scan level and the temporal variability of inferred hail areal extent (HAE). Significant relationships were determined in this study between mean HAE/variability and several environmental parameters. Hail polarimetric radar signatures were also compared across environments; results showed that certain environments produce distinctive mean hail areal extent and hail variability. Correlations between HAE and environment variables are generally higher when the storm has a mean altitude greater than 1 km. An increase in some thermodynamic parameters is observed to produce an increase in mean HAE, while an increase in shear produces an increase in hail variability. Predictive equations for HAE and hail variability are also developed from the analyzed environmental variables.

Acknowledgements

I would like to thank my advisor, Dr. Van Den Broeke for accepting me as a graduate student and for all the support that he has offered. The thoughtful comments and suggestions from my committee members, Dr. Houston and Dr. Anderson, have been appreciated as well. I would also like to thank my fellow graduate students, specifically Sabrina Jauernic, Nicholas Humrich, and Adrienne Engel for help with gathering the environmental data and analysis. Last but not least, the encouragement of family and friends, especially my parents and my sister, has been greatly treasured as well. This research would not have been done without the financial support of the Department of Earth and Atmospheric Sciences in the form of teaching assistantships and NSF grants AGS-1355916 and IIA-1539070.

Table of Contents

Chapter 1. Introduction.....	1
Chapter 2. Background.....	4
<i>I. Supercell Storms.....</i>	<i>4</i>
<i>II. Radar Polarimetry.....</i>	<i>7</i>
<i>III. Polarimetric and Microphysical Features of Supercell Storms.....</i>	<i>11</i>
<i>Polarimetric Features.....</i>	<i>11</i>
<i>Hail Microphysics.....</i>	<i>12</i>
<i>IV. Environmental Variability.....</i>	<i>14</i>
Chapter 3. Methods.....	18
Chapter 4. Environmental Variables.....	27
Chapter 5. Results and Discussion.....	31
<i>I. Thermodynamic Parameters.....</i>	<i>40</i>
<i>MLCAPE.....</i>	<i>40</i>
<i>MUCAPE.....</i>	<i>41</i>
<i>CIN.....</i>	<i>44</i>
<i>LFC Height.....</i>	<i>49</i>
<i>Ambient 0°C Level Height.....</i>	<i>54</i>
<i>LCL Temperature.....</i>	<i>58</i>
<i>II. Moisture Parameters: 1-km RH, 1-3-km mean RH, 3-6-km mean RH, 3-9-km mean RH.....</i>	<i>58</i>
<i>III. Shear Parameters.....</i>	<i>69</i>
<i>0-1-km shear, 0-3-km shear, 0-6-km shear.....</i>	<i>69</i>
<i>ESHEAR.....</i>	<i>77</i>
<i>Storm Relative Helicity: 0-1-km SRH and ESRH.....</i>	<i>81</i>
<i>Hodograph Type.....</i>	<i>82</i>
<i>IV. Predictive Models for HAE and Hail Variability.....</i>	<i>85</i>
Chapter 6. Summary and Conclusions.....	93
References.....	96

MULTIMEDIA OBJECTS

Fig. 2.1: Schematic for a supercell storm (from Moller et al. 1994).....	5
Fig. 2.2: Seven different modes of hail melting (from Rasmussen et al. 1984b).....	14
Fig. 3.1: Non-uniform beam filling (from WDTD 2013).....	19
Fig. 3.2: Approximate storm starting location.....	21
Fig. 3.3: Method of inferring hail areal extent at the base level scan.....	22
Table 3.1: Local variables obtained from archived RUC/RAP model soundings.....	25
Table 4.1: 25 th and 75 th percentiles of variables obtained from RUC/RAP model soundings.....	28
Table 4.2: Environmental variable correlations.....	30
Table 5.1: Independence of cases that occurred on the same day.....	32
Fig. 5.1: Average HAE vs. average HRSV.....	34
Table 5.2: Sample sizes for each defined category.....	35
Table 5.3: Mean hail variability for each category.....	37
Fig. 5.2: Correlation coefficient values for mean HAE vs. selected environmental variables.....	38
Fig. 5.3: Correlation coefficient values for hail variability vs. selected environmental Variables.....	39
Table 5.4: Quartile value for mean HAE and variability value.....	40
Fig. 5.4: Scatter plot for mean HAE vs. MUCAPE for tornadic storms.....	44
Fig. 5.5: Scatter plot for mean HAE vs. CIN for tornadic storms.....	47
Fig. 5.6: Scatter plot for mean HAE vs. CIN for each bin.....	48
Fig. 5.7: Example radar data for variation in mean HAE for CIN environments.....	49
Fig. 5.8: Scatter plot for mean HAE vs. LFC Height for tornadic storms.....	52
Fig. 5.9: Scatter plot for mean HAE vs. LFC Height for each bin.....	53
Fig. 5.10: Example radar data for variation in mean HAE for LFC Height environments.....	54
Fig. 5.11: Scatter plot for mean HAE vs. Ambient Freezing Level Height for nontornadic storms.....	56
Fig. 5.12: Scatter plot for mean HAE vs. Ambient Freezing Level Height for each bin.....	57
Fig. 5.13: Scatter plot for mean HAE vs. 1-km Relative Humidity for tornadic storms.....	60
Fig. 5.14: Scatter plot for mean HAE vs. 1-6-km mean Relative Humidity for tornadic storms.....	62

Fig. 5.15: Scatter plot for mean HAE vs. 3-6-km mean Relative Humidity for nontornadic storms.....	64
Fig. 5.16: Scatter plot for mean HAE vs. 3-6-km mean Relative Humidity for each bin.....	65
Fig. 5.17: Scatter plot for mean HAE vs. 3-9-km mean Relative Humidity for nontornadic storms.....	67
Fig. 5.18: Scatter plot for mean HAE vs. 3-9-km mean Relative Humidity for each bin.....	68
Fig. 5.19: Scatter plot for hail variability vs. 0-1-km shear for tornadic storms.....	71
Fig. 5.20: Example hail variability for 0-1-km shear environments.....	72
Fig. 5.21: Example hail variability for 0-6-km shear environments.....	74
Fig. 5.22: Hail variability plotted over shear space.....	76
Fig. 5.23: Scatter plot for mean HAE vs. ESHEAR for tornadic storms.....	79
Fig. 5.24: Scatter plot for mean HAE vs. ESHEAR for each bin.....	80
Table 5.5: Name and description of hodograph types.....	83
Table 5.6: Summary of dominant hodograph type.....	84
Fig. 5.25: Observed vs. predicted HAE for tornadic storms with a HRSV > 1 km.....	89
Fig. 5.26: Observed vs. predicted HAE for all tornadic storms.....	90
Fig. 5.27: Observed vs. predicted HAE for nontornadic environments with a HRSV > 1 km.....	91
Fig. 5.28: Observed vs. predicted hail variability for nontornadic environments with a HRSV > 1 km.....	92

Chapter 1. Introduction

Dissimilar vertical wind and moisture profiles can lead to different microphysical structures in supercell storms (e.g., Beatty et al. 2008; Van Den Broeke 2014; Davenport and Parker 2015), which should be reflected in their radar presentation. The dual-polarization upgrade to the Weather Surveillance Radar-1988 Doppler (WSR-88D) network across the United States has made it possible to infer scatterer properties such as type, shape, size, and orientation on large spatial and temporal scales. Microphysical processes such as hail growth and melting, which can be indicated by inferred scatterer properties, can greatly influence storm evolution (e.g., van den Heever and Cotton 2004; Kumjian and Ryzhkov 2008; Van Den Broeke 2014). For instance, tornado-genesis and maintenance may be influenced by the thermodynamic contribution of precipitation particles in the rear and forward flanks of supercells (Beatty et al. 2008). Polarimetric radar variables such as reflectivity factor at horizontal polarization Z_{HH} and differential reflectivity Z_{DR} (e.g., Balakrishnan and Zrnić 1990; Herzegh and Jameson 1992; Zrnić and Ryzhkov 1999) can be used to assess these scatterer properties, among other variables. Understanding storm-scale processes and evolution, especially in different environments, is extremely important since supercells produce a disproportionate share of the high-impact severe weather across the United States.

Supercell storms as described by Moller et al. (1994) are examined in this study; both storms that generally remain isolated as well as embedded storms are included. The relatively well-understood polarimetric radar signatures of supercell storms offer a way to test the hypothesis that storms characterized by dissimilar environmental moisture and

shear parameters should exhibit less similarity in inferred hail areal extent (HAE) and hail variability than storms characterized by similar moisture and shear parameters. It is hypothesized that environments with drier layers will be associated with larger mean HAE, as modeling studies (e.g., Rasmussen and Heymsfield 1977; Van Den Broeke 2014) have suggested that drier layers are associated with higher hail mixing ratio and greater evaporative cooling, leading to greater surviving hail mass; this result is also suggested by recent observational studies (e.g., Van Den Broeke 2016). Additionally, an increase in shear should produce a corresponding increase in hail production due to possible seeding of ice particles from nearby storms (e.g., Gilmore et al. 2004; Van Den Broeke et al. 2010).

In this thesis, a large scale attempt is undertaken to quantify HAE inferred at the base-level radar scan under a variety of different environmental conditions. Mean inferred areal extent and variability are compared across different wind and moisture environments to determine the most significant environmental parameters influencing these radar-inferable hail characteristics of supercells. Results from this research should aid in operations, as forecasters may be able to warn more effectively for hail threats in addition to threats for other types of severe weather. From a theoretical and modeling perspective, it is also important to learn more about how supercell microphysics are influenced by environmental variability. Idealized modeling sensitivity studies (e.g., van den Heever and Cotton 2004) indicate that hail size influences not only the type of supercell that develops, as well as how a supercell evolves; therefore it stands to reason that the amount of hail production within supercell storms will also influence storm

evolution. Rasmussen and Straka (1998) also suggest that precipitation may play a key role in the generation of mesocyclones and tornadoes. Additionally, the observations of environmental influence on supercell microphysics with a large sample size, such as in this study, can validate previous modeling studies (e.g., Gilmore and Wicker 1998; Dennis and Kumjian 2014; Van Den Broeke 2014).

Chapter 2. Background

I. Supercell Storms

Supercells are convective storms that contain a strong, deep, and long-lived mesocyclone. The characteristics of a mesocyclone include vertical vorticity of at least 10^{-2} s^{-1} and temporal continuity for tens of minutes throughout a substantial depth of the storm (Moller et al. 1994). There are three main types of supercells: classic, low-precipitation (LP), and high/heavy precipitation (HP). Classic supercells exhibit relatively well-known radar and visual signatures, including a hook echo, bounded weak echo region (BWER), strong reflectivity gradient on the inflow side of the storm, and a sheared updraft column (Moller et al. 1994; Bunkers et al. 2006).

Visual observations of classic supercells often include a precipitation-free base and well-defined wall cloud, which appears as a lowering of the precipitation-free base, from which tornadoes may descend (Moller et al. 1994). Although the inflow bases of classic supercells appear precipitation-free, hail and rain may be falling in the portion of the storm dominated by outflow. Above the precipitation-free base, most precipitation particles are suspended in the lower part of the cell by the updraft. Figure 2.1 shows both a plan view (a) and an idealized view of the storm by a viewer to its east (b). The idealized view of the storm shows the overshooting top, the precipitation free-base, lowered wall cloud, and the outflow portion of the cloud base containing precipitation. Depending on distance from the radar, a radar beam may overshoot the part of the storm containing outflow.

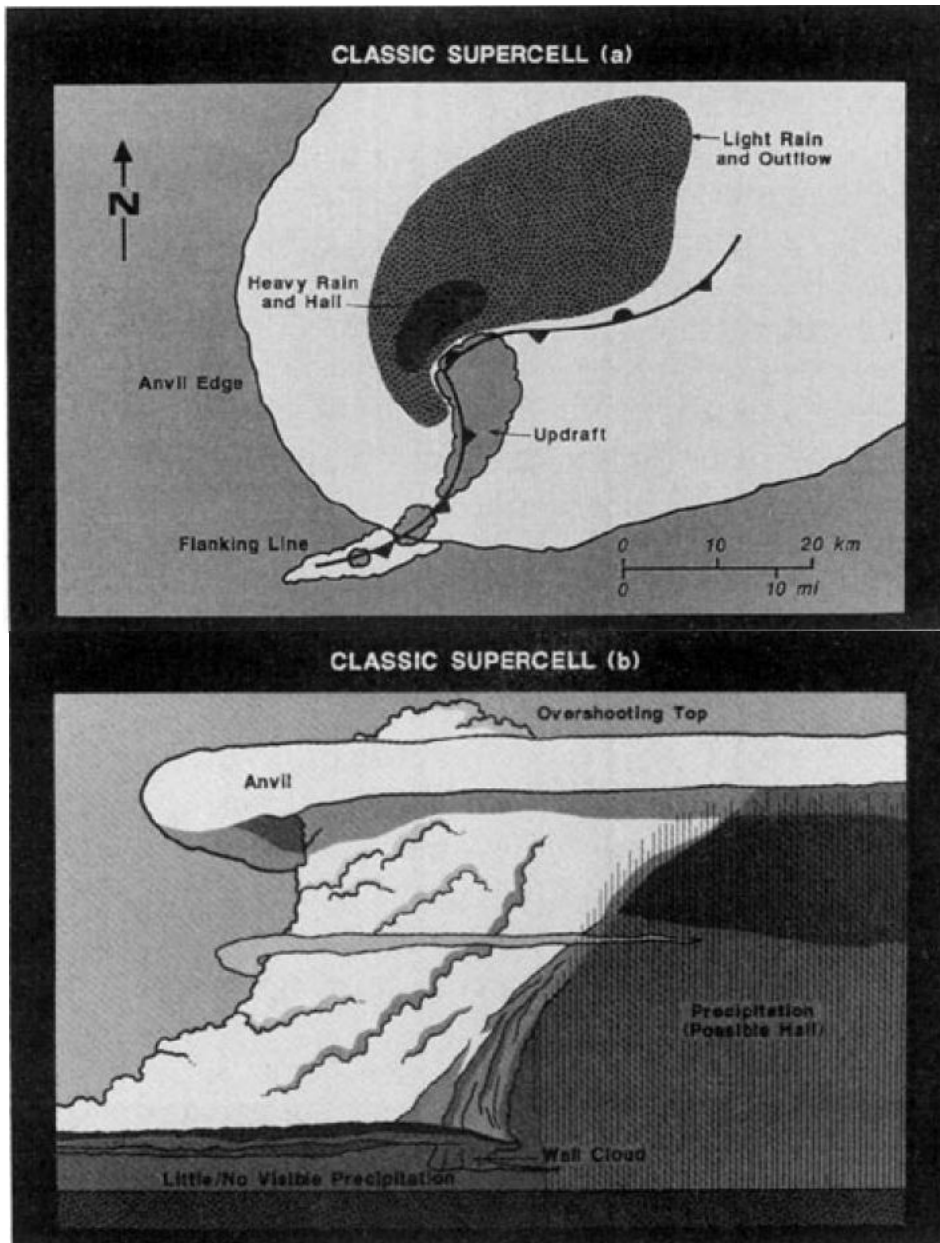


Fig 2.1. Schematics for a classic supercell storm, showing (a) a plan view looking from above showing the precipitation (stippling), surface outflow boundaries (frontal symbols), updraft maxima (scalloped line enclosing the gray area), and cloud boundaries (also scalloped, enclosing white area), and (b) an idealized view of the storm by a surface observer to its east (taken from Moller et al. 1994).

Storm characteristics may vary as a function of environment. LP storms are often characterized by higher levels of free convection, low to moderate values of relative humidity, and strong storm relative (SR) flow at the anvil level (Moller et al. 1994; Rasmussen and Straka 1998). Hail, the most common form of severe weather produced by LP supercells, is the dominant hydrometeor near the updraft of these storms. Rasmussen and Straka (1998) suggest that this is due to the strong SR upper-level flow in these environments; this strong flow transports hydrometeors away from the updraft which reduces the number ingested by the updraft. Meanwhile HP supercells, which may be characterized by enough precipitation in the mesocyclone to obscure rotation, can cause extensive damage through hail and downburst winds (Moller et al. 1994). These storms tend to have a weaker SR upper-level flow, leading to higher precipitation rates as more hydrometeors are ingested by the updraft. Additionally, hail embryos in HP storms may originate from nearby storms and are advected into the updraft (Rasmussen and Straka 1998).

The two most important ingredients for supercells are buoyancy and vertical wind shear (e.g., Lin and Chang 1977; Moller et al. 1994); of these, vertical wind shear is considered more critical for the development of supercells and often comes from locally backed surface winds along thermal boundaries (e.g., Moller et al. 1994). One factor that has been shown to discriminate between storms that have supercellular characteristics and storms with nonsupercellular characters is the bulk wind differential through a deep layer of the atmosphere (e.g., Rasmussen and Blanchard 1998; Thompson et al. 2003; Houston et al. 2008). The discrimination between tornadic and nontornadic supercells

can also be related to bulk wind differential (e.g., Thompson et al. 2012). The strength of the vertical wind shear has also been shown to influence the intensity of the up- and downdrafts within a storm, while magnitude of veering or backing with height determines the location of these features within a storm (e.g., Lemon 1977; Lin and Chang 1977).

Supercells have a cyclic lifecycle, the dominant mode of which is determined by environmental factors (e.g., Gilmore and Wicker 1998; Adlerman and Droegemeier 2005). Supercell demise also has a direct relationship to the storm-relative environment, tending to occur when the storm enters an environment that is too stable or which favors another convective mode. Supercells can also dissipate when they interact with other thunderstorms and when their supply of buoyant, moist inflow is cut off, whether due to other thunderstorms or its own downdraft (Bunkers et al. 2006).

II. Radar Polarimetry

Radar reflectivity at horizontal polarization (Z_{HH}) is a measure of the amount of radiation backscattered to the radar or a measure of the amount of power returned to the radar from both hydrometeors and non-meteorological scatterers in the horizontal direction (Doviak and Zrnić 1993). Z_{HH} depends on particle size, composition, phase (e.g., the dielectric constant) and the radar wavelength (Kaltenboeck and Ryzhkov 2013). Typically, larger particles in the Rayleigh scattering regime have higher reflectivity as there is a larger cross-section to backscatter radiation to the radar. However, the dielectric constant of the hydrometeor is also important to consider when determining an expected Z_{HH} value. Since ice has a smaller dielectric constant than liquid water, an ice

hydrometeor of a given size will have a lower reflectivity than a water hydrometeor of the same size (e.g., Straka et al. 2000). Particle size and phase are important when considering hail, as both the size and water content of hail can vary substantially.

Another factor that may substantially impact polarimetric radar variable values when looking at hail is Mie scatter (Doviak and Zrníć 1993). In the Mie scattering region, the backscattering cross-sectional area of the target can decrease as size increases for certain particles (Rinehart 1991). The effects of Mie scattering typically become significant when the following ratio approximately equals unity:

$$\frac{D|\varepsilon|^{\frac{1}{2}}}{\lambda} \quad (1)$$

where D is the spherical diameter of the particle (cm), ε is the dielectric constant of the particle, and λ is the radar wavelength (cm) (Kumjian and Ryzhkov 2008; Kennedy et al. 2014). According to Kennedy et al. (2014), this ratio becomes unity at a diameter of approximately 5.6 cm for a hailstone composed of solid ice and not containing a liquid water component or air cavities when using a 10-cm radar wavelength. Both Z_{HH} and Z_{DR} can be affected by this difference in scattering regimes, as a smaller or larger amount of power may be returned to the radar than expected by scatterers in the Mie regime, decreasing or increasing the Z_{HH} and differential reflectivity (Z_{DR}) values.

The introduction of dual-polarization capabilities to weather radars has allowed for the collection of variables that have proven useful for hydrometeor identification when combined with reflectivity factor; however, radar reflectivity from singularly-polarized radars has been used to infer specific hydrometeors (such as hail) as early as the

late 1950s (Heinselman and Ryzhkov 2006). Variables useful for hydrometeor identification include Z_{HH} , Z_{DR} , and the co-polar cross-correlation coefficient (ρ_{hv}), among others. The information provided from each of these variables, although important on their own, can provide more insight regarding the type of scatterer when combined (e.g., Doviak and Zrnić 1993; Straka et al. 2000; Park et al. 2009). The WSR-88D network provided Z_{HH} before the dual-polarization upgrade; however, the availability of variables such as Z_{DR} has come after the upgrade as these variables take into account both horizontal and vertical polarization. Z_{HH} and Z_{DR} are briefly defined here, with an emphasis on their physical interpretation. Readers are referred to other sources such as Balakrishnan and Zrnić (1990), Herzegh and Jameson (1992), and Zrnić and Ryzhkov (1999) for more complete descriptions of these variables.

Z_{DR} is the logarithmic ratio of the linear reflectivity in the horizontal and vertical directions, also described as the difference between the logarithmic reflectivity in the horizontal and vertical directions:

$$Z_{DR} = 10 \cdot \log_{10} \frac{Z_{HH}}{Z_{VV}} \quad (2)$$

$$Z_{DR} = Z_{HH} - Z_{VV} \quad (3)$$

Since chaotically tumbling hydrometeors such as hailstones appear as spheres to the radar in the mean (and therefore the horizontal reflectivity factor (Z_{HH}) equals the vertical reflectivity factor (Z_{VV})), the Z_{DR} in hail regions appears to be ~ 0 dB or are at least local minima within the storm (Doviak and Zrnić 1993; Heinselman and Ryzhkov 2006; Kumjian 2011). However, small melting hail can have Z_{DR} values as high as 5-6 dB as it appears to the radar as large raindrops (WDTD 2013). The hailfall region

appears to be collocated or very close to the maximum Z_{HH} values (Doviak and Zrnić 1993). Z_{DR} is also dependent on the shape, size, orientation, density, and water content of the specific collection of scatterers, although this polarimetric variable is independent of particle concentration (Kumjian 2011). For example, water coated melting hail might have slightly higher Z_{DR} when compared to dry hail due to its more stable orientation, and giant hail (diameter > 5 cm) may exhibit slightly negative Z_{DR} values due Mie scattering (Kaltenboeck and Ryzhkov 2013). According to Kumjian and Ryzhkov (2008), one common indicator of hail reaching the ground is high reflectivity factor collocated with near-zero Z_{DR} at the lowest elevation angle. The collocation of these values above the freezing level also indicates hail aloft (e.g., Zrnić and Ryzhkov 1999).

Classification schemes such as the hydrometeor classification algorithm (HCA) combine information that is obtained from polarimetric variables, such as Z_{HH} , Z_{DR} , and ρ_{hv} using a fuzzy logic classification scheme (e.g., Heinselman and Ryzhkov 2006; Park et al. 2009). To classify hydrometeors, fuzzy logic algorithms take the polarimetric variables as inputs, assign probabilities to each type of hydrometeor for each variable based on a set of weighted rules, and choose the hydrometeor species with the highest resultant likelihood (e.g., Liu and Chandrasekar 2000; WDTD 2013). The HCA assigns a membership function, or a range of values typically observed in each polarimetric variable (such as those described in Straka et al. 2000), to be associated with each class of radar echo (e.g., hail is associated with $55 \text{ dBZ} < Z_{HH} < 80 \text{ dBZ}$ in the HCA at S-band). Weights are assigned to each variable based on the efficiency the variable has in discriminating each class of hydrometeor, and the HCA chooses the most likely

hydrometeor class. The weight assignment and the weighting matrix used by the WSR-88D network is presented by Park et al. (2009). Z_{DR} is the most important variable used by the HCA to identify graupel, so it is given a weight of 1.0; other variables such as ρ_{hv} that are not as important are given lower weights.

III. Polarimetric and Microphysical Features of Supercell Storms

Polarimetric Features

Various observational and modeling studies have found hail fallout in repeatable locations within supercell storms. Large hail is often associated with supercell events (e.g., Bunkers et al. 2006) and has been observed just downstream from the mesocyclone (e.g., Moller et al. 1994; Hubbert et al. 1998; Van Den Broeke et al. 2008). However, these hail signatures may also appear in the echo appendage, near the edges of the mesocyclone as previous studies have noted hail observations as well as hail polarimetric signatures in these regions (e.g., Browning 1965; Auer 1972; Finley et al. 2001; Van Den Broeke 2014, 2016). Z_{HH} and Z_{DR} have been used to qualitatively infer that hail is present most commonly at times leading up to tornadogenesis (Van Den Broeke et al. 2008). Hailfall has also been seen to occur more frequently at the time of tornadogenesis when compared to pre-tornado times or times after tornado demise (Van Den Broeke et al. 2008; Kumjian and Ryzhkov 2008). Kumjian and Ryzhkov (2008) found that in most of the tornadic cases in their sample, the status of the hail signature (whether it was present or absent) in the time leading up to tornadogenesis remained the same after tornadogenesis. They also found hail signatures to be more intermittent in tornadic

supercells, suggesting cyclic hailfall, while nontornadic storms display more persistent hail signatures (Kumjian and Ryzhkov 2008; Van Den Broeke 2016). The authors speculate that this is due to the weakening of the tornadic supercell updraft around the time of tornadogenesis to the extent that hail production is lessened, and propose that the persistence of hail can provide insight into the tornadic potential of a supercell storm. Simulations of supercell storms show that hodograph shape may influence the placement of hail. Van Den Broeke et al. (2010) show that in simulations with a half-circle hodograph, hail tended to be confined to the storm core. Meanwhile in simulations with full-circle hodographs, hail tended to spread southward and wrap around the west side of the mesocyclone (Van Den Broeke et al. 2010).

Hail Microphysics

Hail is formed when either graupel or frozen drops accrete supercooled drops, and recent models show that hail formed from these embryos can occur north of the updraft region (Rogers and Yau 1996; Van Den Broeke 2014). Browning and Foote (1976) developed a three-stage model for the growth of hail in a supercell: 1) hail embryos are grown through a first ascent within weaker storm updrafts, 2) some of the embryos are advected away from the main updraft and either evaporate or fall out while some of the embryos reach the forward edge of the updraft while descending, and 3) these embryos re-enter the main updraft and continue growing until the hailstones cannot be supported by the updraft. Browning and Foote note, though, that “not all of the embryos re-entering the main updraft can be expected to grow into large hailstones; many may quickly

encounter intense updrafts and be carried above the -40°C level before they had time to grow quickly.”

The melting of hail is closely related to latent heat transfer and the cloud water distribution (Rasmussen et al. 1984 a,b; Rasmussen and Heymsfield 1987). Rasmussen et al. (1984b) defined seven different melting modes for hail (Fig. 2.2), depending on the size of the melting hailstone. The drops shed by hail during these modes can lead to characteristic drop size distributions (DSDs) as the DSDs change from this process; additionally, latent heat released through this process has major implications for the storm’s energy budget via evaporative cooling. In idealized simulations, van den Heever and Cotton (2004) showed that hail size has an impact on low-level dynamic and thermodynamic characteristics such as downdraft and cold-pool strength. This agrees with Srivastava (1987), who showed that the cooling of the downdraft is influenced by the melting of the ice phase. These microphysical processes associated with hail impact storm morphology and evolution; in order to better understand how supercells evolve, these microphysical processes and their response to environmental variability need to be better comprehended.

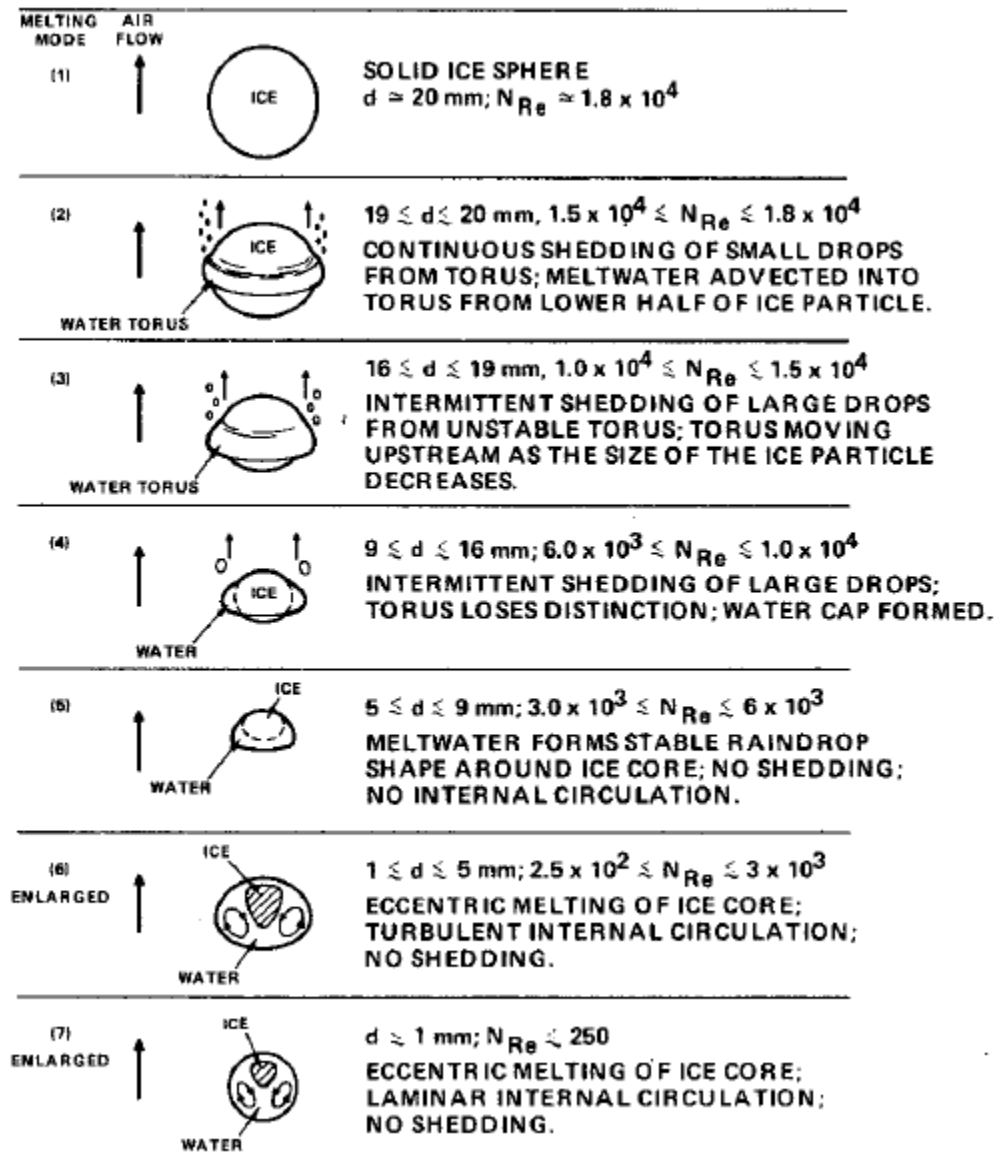


Fig. 2.2: Seven different modes of hail melting (taken from Rasmussen et al. 1984b).

IV. Environmental Variability

Research has shown that certain environmental variables influence supercell formation and demise. Observational studies (e.g., Shabbot and Markowski 2006; Parker 2014, among others) have provided evidence for how supercell characteristics differ as a

function of environmental variability from either mesonet or sounding observations. These studies, as well as Markowski et al. (1998), show that representing the storm environment using a single sounding can introduce error as there can be large environmental variability occurring on small spatial scales in the vicinity of supercells. Some of the problems associated with understanding such environments include what time and space scales represent storm environments (Brooks et al. 1994). Model output soundings such as those from RUC/RAP have the advantage of a “superior spatial and temporal resolution compared to that of the upper-air observing network across the United States” (Thompson et al. 2003). Error analysis, as described by Thompson et al. (2003), showed that while outputs tended to be a little too dry and cool at the surface, temperature, moisture and wind speed errors tended to be of similar magnitude to those of radiosonde measurements. Additionally, even though the mixed layer convective available potential energy (MLCAPE) was over-forecast, errors were too small to have a significant impact on evaluation of storm environments. Benjamin et al. (2016) also showed that there are errors on the order of 2-3°C for low-level dewpoints when RAP outputs are verified against METAR observations. This caveat should be noted when looking at the environmental variables, as the dewpoint error could influence the moisture and instability indices recorded and calculated.

The production of hail is also dependent on different environmental factors, most of which are related to wind or moisture. Van Den Broeke (2016) showed that the 51.2% of the mean base-scan HAE (km^2) can be predicted using the equation

mean base scan HAE (km²) =

$$7.527 + 1.31 \cdot 10^{-2}(a) - 2.41 \cdot 10^{-1}(b) - 6.36 \cdot 10^{-2}(c) \quad (4)$$

where a is the height of the level of free convection (LFC; m), b is 6-km relative humidity (RH; %) and c is convective inhibition (CIN; J kg⁻¹). Higher LFC heights, which had a positive correlation to mean HAE ($r = 0.55$) was thought to be associated with an increase in hail production as the updrafts were colder due to their higher altitude. 6-km RH had a negative correlation to HAE ($r = -0.58$), which supported previous studies. Simulated storms show that the amount of drying within a layer has an effect on the amount of hail produced in a particular storm (Rasmussen and Heymsfield 1987; Van Den Broeke 2014). When layers are drier, a greater amount of hail may survive to reach low levels, since hailstones falling through drier air experience greater evaporative cooling, leading to less melting (Rasmussen and Heymsfield 1987). Similarly, altitude of the 0°C level was hypothesized to be important for HAE as melting closer to the surface would suggest more hail mass survives. Additionally, it has previously been shown that convective inhibition (CIN) can be a predictor of hailstorms (Foote and Wade 1982; Colby 1984).

Simulations have also shown that hail mixing ratio is cyclic in supercell storms (Van Den Broeke 2014), consistent with earlier observational results (e.g., Kumjian et al. 2008; Van Den Broeke et al. 2008). Thus, hail production is thought to be tied to mesocyclone cycling and updraft pulses (Adlerman and Droegemeier 2005; Van Den Broeke 2010). Van Den Broeke (2016) looked into the predictability of hail variability by environment. Variability is defined as the coefficient of variation as in Van Den

Broeke (2016). The coefficient of variation is calculated by dividing the standard deviation of the measured value by the mean measured value (Everitt 2002):

$$c_v = \frac{\sigma}{\mu} \quad (5)$$

99.3% of hail variability was found to be predicted by the following equation:

$$c_v = 0.7522 + 2.4 \cdot 10^{-4}(a) - 6.22 \cdot 10^{-4}(b) + 3.73 \cdot 10^{-3}(c) - 3.11 \cdot 10^{-2}(d) \quad (6)$$

where a is MLCAPE (J kg^{-1}), b is effective storm relative helicity (ESRH; $\text{m}^2 \text{s}^{-2}$), c is mean 3-9-km RH (%), and d is lifting condensation level (LCL) temperature ($^{\circ}\text{C}$). LCL temperature should be significant to hail production since colder LCLs can indicate colder updrafts; Van Den Broeke (2016) presented no speculations on how this thermodynamic parameter would be related to hail variability and noted that 97% of variability could be explained without using LCL temperature. The positive relationship between variability of mean areal extent and MLCAPE ($r = 0.34$) was suggested to be due to a relationship between ambient instability and updraft characteristics such as speed.

Chapter 3. Methods

The polarimetric radar dataset of storms was constructed generally following the approach of Thompson et al. (2003). Severe weather reports were identified near a polarimetric WSR-88D from February 2012-December 2014 using the Storm Events Database from the National Centers for Environmental Information (NCEI; NOAA 2014b). On a day with storm reports, supercell storms were identified using the criteria of Thompson et al. (2003), including one or more radar reflectivity structures characteristic of supercells (e.g., a hook echo, inflow notch, weak echo region, and/or V notch as suggested by Browning (1965) and Lemon (1977)), the cyclonic azimuthal shear in the lowest two elevation angles met the threshold value for mesocyclones defined by Stumpf et al. (1998), and this cyclonic shear persisted for at least 30 minutes. This time constraint ensures that at least 7 time steps are included in the analysis of every storm, which allows a representative mean HAE to be calculated.

Supercell storms were also required to be within ~125 km of a WSR-88D to ensure high quality polarimetric data for several reasons. Beam filling influences weather radar data quality, especially with increases in range (WDTD 2013). At large ranges, the beam is filled with a mix of hydrometeors; this non-uniform beam filling negatively impacts certain dual-polarimetric products as it can produce a gradient of precipitation types within the beam (Fig. 3.1). This implies that even though hail is identified through multiple dual-pol products, at long ranges there might be other hydrometeors sampled. This is especially true when sampling a convective storm at large range or a squall line that is directly down radial from the radar (WDTD 2013).

Horizontal and vertical resolutions are also reduced at large ranges since the area that the beam samples at large ranges is greater than the area sampled close to the radar. Finally, hail extent needs to be estimated fairly close to the ground in order to make the assumption that inferred hail extent at the base-level scan reached the ground; this precluded storms at large range.



Fig. 3.1: A non-uniform mixture can produce a gradient of precipitation types within a radar beam (black circle). Mostly hail is sampled at the top of the beam, the middle is sampling rain and wet hail, and the bottom of the beam is sampling rain only (taken from WDTD 2013).

The resulting dataset consisted of approximately 145 cases and included both environments that produced tornadic supercells (94 cases; 65%) and nontornadic

supercells (51 cases; 35%); these storms were selected without preference for geographic region (Fig. 3.2), though more Great Plain storms were selected due to the prevalence of supercell storms in that geographic region. For each supercell identified, level II radar data from the nearest WSR-88D were obtained from NCEI (NOAA 2014a). The radar data were imported into NCEI's Weather and Climate Toolkit, and differential reflectivity (Z_{DR}) data were then converted to shapefiles for analysis. Z_{DR} data were thresholded between -0.5 dB and 1 dB for hail as in previous studies (e.g., Doviak and Zrnić 1993; Heinselman and Ryzhkov 2006; Kumjian 2011; Kaltenboeck and Ryzhkov 2012). The locations of thresholded values of Z_{DR} were manually compared with locations of high Z_{HH} (> 55 dBZ), a common indicator of hail reaching the ground (Kumjian and Ryzhkov 2008; WDTD 2013). Hail was inferred to be present where Z_{DR} values within the thresholding range are collocated with high Z_{HH} values within the storm core, and the inferred HAE was measured (Fig. 3.3). It should be noted that the mean HAE may depend on storm size, which could be defined as the area enclosed by the 35-dBZ contour, though this factor was not controlled for in this study.



Fig. 3.2: Approximate starting locations for supercellular storms. Nontornadic storms are represented with black dots and tornadic storms are represented with red dots.

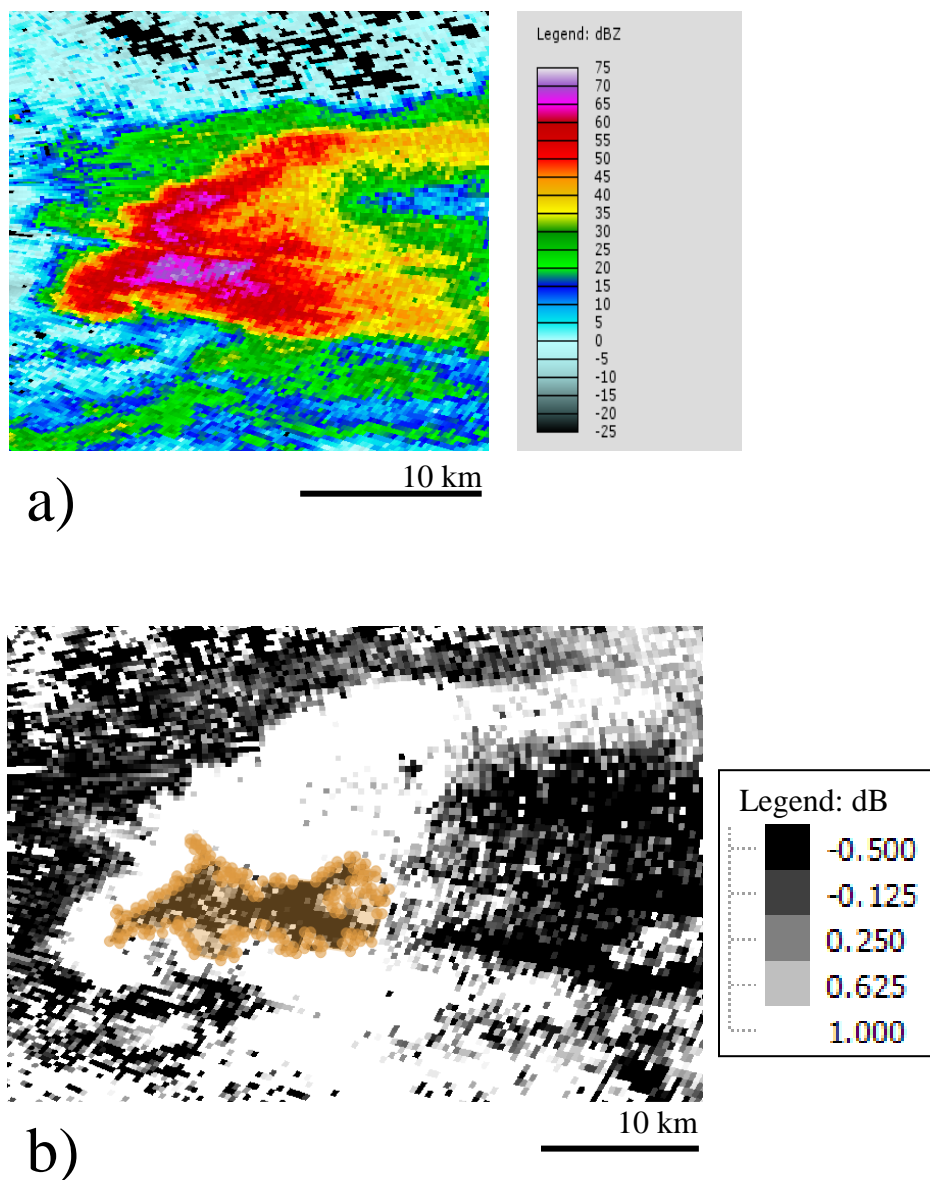


Fig. 3.3: Method of inferring HAE at the base-level scan for sample storm in the domain of KGGW (Glasgow, Montana) on 24 July 2013 at 2202 UTC. A) Reflectivity factor at horizontal polarization (Z_{HH}). B) Differential reflectivity (Z_{DR}) thresholded between -0.5 dB and 1 dB. The tan area represents inferred hail that meets both the reflectivity ($Z_{HH} > 55$ dBZ) and differential reflectivity ($-0.5 \text{ dB} < Z_{DR} < 1 \text{ dB}$) criteria.

Archived Rapid Update Cycle (RUC) and Rapid Refresh (RAP) model output, available from the National Operational Model Archive and Distribution System (NOMADS; Karsten 2010), were used to provide proximity environmental data, as similar data have been used successfully to represent near-storm environments (Thompson et al. 2003, 2007). Sites for which model soundings were available were identified within ~80 km of each storm and the midpoint of the analysis period. Surface, satellite, and radar observations are utilized to ensure that the sites were representative of the air mass in which the storm is located (e.g., on the same side of mesoscale boundaries, and in a region representative of storm inflow). In rare cases, no sites were representative of the storm as there are boundaries in the area, convective contamination, or no nearby locations, and the storm was discarded.

Table 3.1 shows the local variables obtained from the archived RUC/RAP soundings, which represent the local thermodynamic environment and vertical moisture/wind profiles. These environmental variables overlap those assessed in prior work (e.g., Rasmussen and Blanchard 1998; Rasmussen 2003; Thompson et al. 2003). If two RUC/RAP soundings were obtained for an event (e.g., a 12 UTC and 13 UTC soundings for a 1230 UTC event), the two values obtained for a given variable were averaged in order to obtain representative values. Mean relative humidity for a layer was calculated using pressure weighting, as in the following equation:

$$\text{Mean RH (\%)} = \frac{RH_B * \ln(P_B) + RH_T * \ln(P_T)}{\ln(P_B + P_T)} \quad (7)$$

where RH_B and RH_T are the values of relative humidity at the bottom and top of the layer respectively (%), and P_B and P_T are the pressure associated with the bottom and top of the

layer respectively (mb). This calculation weights the relative humidity toward the part of the layer with higher density, and is especially important at upper levels.

Table 3.1: Local variables obtained from archived RUC/RAP soundings.

Classification	Variable
Thermodynamic Parameters	MLCAPE (J kg^{-1})
	MUCAPE (J kg^{-1})
	CIN (J kg^{-1})
	LFC Height (m)
	Ambient 0°C Level (m)
	LCL Temperature ($^\circ\text{C}$)
Moisture Parameters	6 km Relative Humidity (%)
	3-6 km Mean Relative Humidity (%)
	3-9 km Mean Relative Humidity (%)
Shear Parameters	0-1 km bulk shear (kt.)
	0-3 km bulk shear (kt.)
	0-6 km bulk shear (kt.)
	Effective bulk shear (kt.)
	0-1 km storm relative helicity ($\text{m}^2 \text{s}^{-2}$)
	0-3 km storm relative helicity ($\text{m}^2 \text{s}^{-2}$)
	Effective storm relative helicity ($\text{m}^2 \text{s}^{-2}$)
Hodograph Parameters	General hodograph type: Linear, Curved, Segmented

The Wilcoxon-Mann-Whitney (WMW) rank-sum test was employed to determine which differences in average inferred HAE and hail variability are statistically significant across environments. The WMW test, a non-parametric test which indicates whether two means come from different populations, tests the one-tailed or two-tailed null hypothesis that two samples come from different populations (Wilks 2011). This nonparametric test is used, as no assumptions were made about the distributions of the data, and some groups being compared were relatively small. Unless otherwise stated, all WMW tests were run at the 5% confidence level and were run testing the two-tailed null hypothesis since no assumptions were made about which sample should have a larger mean value (Wilks 2011).

Chapter 4. Environmental Variables

Values representative of the near-storm environment were obtained or calculated from RUC/RAP model soundings as in Thompson et al. (2003, 2007). These variables, found in Table 4.1, overlap those assessed in prior work (e.g., Rasmussen and Blanchard 1998; Rasmussen 2003; Thompson et al. 2003). The 25th and 75th percentiles were calculated for all variables and these were compared to values in previous studies (e.g., Rasmussen and Blanchard 1998; Rasmussen 2003; Thompson et al. 2003, 2007). It was determined that the calculated values were representative of supercell environments. These percentiles were also used to describe low (less than 25%) and high (greater than 75%) environments while running the Wilcoxon-Mann-Whitney p -test in order to see if there were statistical differences between environments. Correlations were also run between the analyzed variables which were investigated in more detail (Table 4.2). After environmental analysis, the Belsley condition index (Belsley et al. 2005) was used to check the collinearity between variables in order to remove linearly dependent variables from the developed predictive equations. Variables that had a condition index value greater than 30 were removed from the predictive equations.

Table 4.1: Variables (and units) obtained from archived RUC/RAP model soundings.

The 25th and 75th percentile values are shown for each variable.

Variable (Units)	25th percentile	75th percentile	Reference
MLCAPE (J kg^{-1})	190.5	1413.5	Evans and Doswell (2001); Thompson et al. (2003)
MUCAPE (J kg^{-1})	621	1740.5	Evans and Doswell (2001)
CIN (J kg^{-1})	9	87	Foote and Wade (1982); Colby (1984); Rasmussen and Blanchard (1998)
0-1 km Shear (kt.)	8	17	Thompson et al. (2003)
0-3 km Shear (kt.)	19	33	Thompson et al. (2003)
0-6 km Shear (kt.)	31.5	49	Thompson et al. (2003)
ESHEAR (kt.)	23	35.5	Thompson et al. (2007)
0-1 km SRH ($\text{m}^2 \text{s}^{-2}$)	44.5	242.5	Rasmussen and Blanchard (1998); Rasmussen (2003)
0-3 km SRH ($\text{m}^2 \text{s}^{-2}$)	92.5	334	Rasmussen and Blanchard (1998); Rasmussen (2003)
ESRH ($\text{m}^2 \text{s}^{-2}$)	70	255	Thompson et al. (2007)
LCL Height (m)	308.5	1125.5	Rasmussen and Blanchard (1998)

LFC Height (m)	1164	2646	
LCL Temp (°C)	13.5	19.5	
0°C Height (m)	3000	3850	
1 km RH (%)	64.3	95.8	
3 km RH (%)	40.3	90.3	
6 km RH (%)	9.3	65.79	
9 km RH (%)	18.2	66.6	
1-3 km mean RH (%)	59.6	84.1	
3-6 km mean RH (%)	32.9	70.4	
3-9 km mean RH (%)	37.9	70	
6-9 km mean RH (%)	19.12	63.2	
SCP	0.1	0.5	Thompson et al. (2003)
STP	0.1	1.4	Thompson et al. (2003)
EHI	0.02	1.1	Rasmussen (2003)

	MUCAPE	CIN	LFC Height	Ambient 0°C Height	LCL Temperature	1 km RH	6 km RH	1-3 km Mean RH	3-6 km Mean RH	3-9 km Mean RH	0-1 km Bulk Shear	0-3 km Bulk Shear	0-6 km Bulk Shear	ESHEAR	0-1 km SRH	0-3 km SRH	ESRH
MUCAPE	0.88	-0.19	-0.31	0.17	0.32	0.14	-0.14	-0.07	-0.21	-0.21	-0.21	-0.21	-0.14	0.30	-0.15	-0.16	-0.02
MUCAPE		-0.11	-0.14	0.23	0.38	0.07	-0.09	-0.07	-0.15	-0.16	-0.18	-0.14	-0.11	0.28	-0.11	-0.10	0.06
CIN			0.70	-0.05	0.02	-0.28	0.12	-0.34	-0.04	-0.16	0.32	0.39	0.35	0.18	0.17	0.26	0.01
LFC Height				-0.06	-0.17	-0.45	0.08	-0.38	0.01	-0.05	0.13	0.24	0.24	-0.03	0.07	0.17	-0.05
Ambient 0°C Height					0.56	0.08	0.08	0.12	0.12	0.14	-0.02	-0.10	-0.15	-0.09	-0.07	-0.11	-0.16
LCL Temperature						0.36	0.06	0.28	0.08	0.07	0.04	-0.01	-0.04	0.08	0.02	-0.03	-0.04
1 km RH							0.02	0.69	0.08	0.18	0.25	0.18	0.22	-0.12	0.34	0.25	0.21
6 km RH								0.18	0.82	0.50	0.09	0.03	-0.06	0.12	0.03	-0.01	-0.05
1-3 km Mean RH									0.60	0.70	0.10	0.02	0.01	-0.29	0.23	0.17	0.20
3-6 km Mean RH										0.81	0.01	-0.07	-0.17	-0.08	0.02	0.00	-0.01
3-9 km Mean RH											0.01	-0.04	-0.15	-0.17	0.12	0.09	0.06
0-1 km Bulk Shear												0.86	0.80	0.23	0.82	0.75	0.62
0-3 km Bulk Shear													0.92	0.36	0.71	0.80	0.66
0-6 km Bulk Shear														0.41	0.67	0.74	0.63
ESHEAR															0.22	0.26	0.24
0-1 km SRH																0.90	0.74
0-3 km SRH																	0.80

Table 4.2: Correlations between a subset of environmental variables that were further investigated. Correlation values greater than

0.50 are bolded.

Chapter 5. Results and Discussion

After storms were discarded due to a lack of representative sites, the storms were categorized as having occurred in tornadic environments or nontornadic environments. Nontornadic and tornadic categories were determined from NCEI's Storm Events Database, although this source may have omitted a weak tornado. NCEI's Storm Events Database was also utilized in order to confirm that storms in tornadic environments produced a tornado; if no tornado was produced, the storm was discarded. This resulted in a final dataset consisting of 123 storms, 40% ($n = 49$) of which were nontornadic and 60% ($n = 74$) of which were tornadic. Independence of storm environments was examined within the dataset; first, each separate event had its own unique sounding, which helps establish independence. Additionally, the number of events from the same day and region were quantified. It is seen that 89 of the storms (72%) occurred on separate days, while the remaining cases were divided into 13 different sets of cases that occurred on the same day (Table 5.1). If the soundings for the storms in these cases were farther apart than 100 km, it was determined that these cases were spatially independent. It was observed that for events occurring on the same day in the same general region, their environments were observed to be independent.

Table 5.1: Independence of cases that occurred on the same day. Asterisks denote cases that contained storms that were both spatially independent and non-spatially independent. In these cases, the first number in the second column is the number of cases that are not spatially independent.

Day	Number of Cases	Independent by Space (> 100 km between soundings)	Independent by Environmental Profile
2 March 2012*	2/1	No/Yes	Yes
14 April 2012	2	Yes	
2 February 2013	2	No	Yes
18 March 2013	2	Yes	
31 March 2013	2	No	Yes
11/12 April 2013	2	No	Yes
20 May 2013*	2/5	No/Yes	Yes
27 May 2013	2	Yes	
17 June 2013	3	Yes	
18 June 2013	2	Yes	
15 August 2013	2	No	Yes
17 November 2013	3	Yes	
20 May 2014	2	Yes	

While analyzing the data, the mean height of the hail core at the base-level scan was recorded for each time step in order to calculate the mean height of the radar sample volume (HRSV). This metric was also used to categorize storm data in order to separately consider storms with a mean HRSV below 1 km and storms with a mean HRSV above 1 km in height. These separate height categorizations were needed as the HRSV increases as the beam travels farther from the radar:

$$h = [r^2 + (k_e a)^2 + 2rk_e a \cdot \sin(\theta_e)]^{\frac{1}{2}} - k_e a \quad (8)$$

where h is the height of the radar beam, r is the range from the radar, a is the radius of the earth, k_e is the constant 4/3, and θ_e is the elevation angle (Doviak and Zrnić 1993). This is important from the perspective of hail. More hail might be present with greater altitude due to melting at low levels. Additionally, HAE at the HRSV may not match HAE on the ground as melting might occur between the scan altitude and ground level. The presence of melting hail can modify low-level thermodynamic environments, which can in turn modify storm evolution (e.g., Van Den Broeke 2014). As the mean HRSV increases, so does the measured inferred HAE (Figure 5.1). Approximately 12% of the variability of HAE is explained by HRSV.

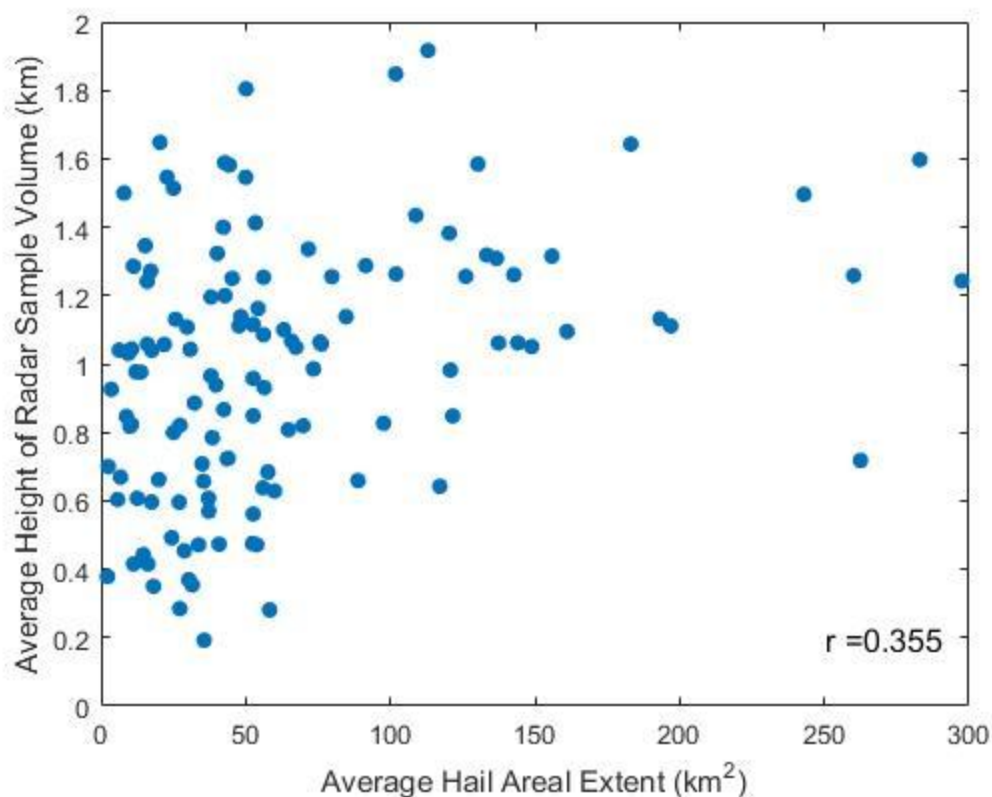


Figure 5.1: Average HAE (km^2) vs. average HRSV (km). As the average height of the radar sample volume increases, the average areal extent of inferred hail also increases slightly.

Table 5.2 shows the sample sizes from the categories that were developed when the storms were subdivided by mean HRSV and tornadic/nontornadic status. For the Wilcoxon-Mann-Whitney p -tests, the environmental variables were broken into the lowest 25% of values for the entire dataset (LOW), the middle 50% (MID), and the highest 25% (HIGH) in order to see if there was a statistical difference between LOW and HIGH environments (e.g., if hail extent and variability that occurred in LOW-CAPE

environments were different than those that occurred in HIGH-CAPE environments), and to see if extreme events are associated with particular hail characteristics (e.g., are LOW-CAPE environments different than both MID- and HIGH-CAPE environments).

Nontornadic storms with mean HRSV below and above 1 km, tornadic storms with mean HRSV below and above 1 km, and all storms with mean HRSV below and above 1 km were all used to calculate p -values.

Table 5.2: Sample sizes and percent of total storms analyzed for each defined category.

Category	n	% of total
Nontornadic below 1 km	22	18
Nontornadic above 1 km	27	22
Tornadic below 1 km	37	30
Tornadic above 1 km	37	30
All Storms below 1 km	59	48
All Storms above 1 km	64	52

The variability in mean inferred HAE, measured by the coefficient of variation, was also calculated for each storm. Values range from 0.162 (variations in HAE were quite small relative to the mean) to 1.314 (variations in HAE exceeded the mean value). Mean hail variability does not differ substantially between tornadic storms (mean coefficient of variation = 0.56) and nontornadic storms (mean coefficient of variation = 0.62); this result appears to be in contrast with results Van Den Broeke (2016). Kumjian

and Ryzhkov (2008) also found that tornadic storms have more variability; however, they compared the frequency of the presence of hail signatures throughout the mature lifetime of the storm. This study does not take into account when the variability, with respect to the mean, takes place within the lifetime of a particular storm. Van Den Broeke et al. (2008) found that tornadic storms showed high variability of hailfall at low levels, while low variability occurs in nontornadic storms at low levels. It was speculated that lower-level samples would generally have larger mean hail variability; however, there was also no substantial difference in mean hail variability based on the mean HRSV of the storm (Table 5.3).

Table 5.3: Mean hail variability for each category.

Height	Tornadic/Nontornadic	Mean Coefficient of Variation
Below 1 km	Nontornadic	0.66
	Tornadic	0.56
	All Storms	0.60
Above 1 km	Nontornadic	0.58
	Tornadic	0.55
	All Storms	0.56
Any altitude	Nontornadic	0.62
	Tornadic	0.56
	All Storms	0.58

Analyses were performed on each subset of data to determine correlation coefficients between 1) the mean hail areal extent of storms within a subset to corresponding values of environmental variables hypothesized to influence the *hail areal extent* (Fig. 5.2) and b) the variability of hail areal extent of storms within a subset to corresponding environmental variables hypothesized to influence the *variability of hailfall* within supercell storms (Fig. 5.3). If the correlation coefficient was substantial ($|r| \geq 0.4$), areal extent and variability were divided into quartiles (Table 5.4) in order to determine if an environmental variable was strongly correlated to hail characteristics within a specific range of HAE or variability.

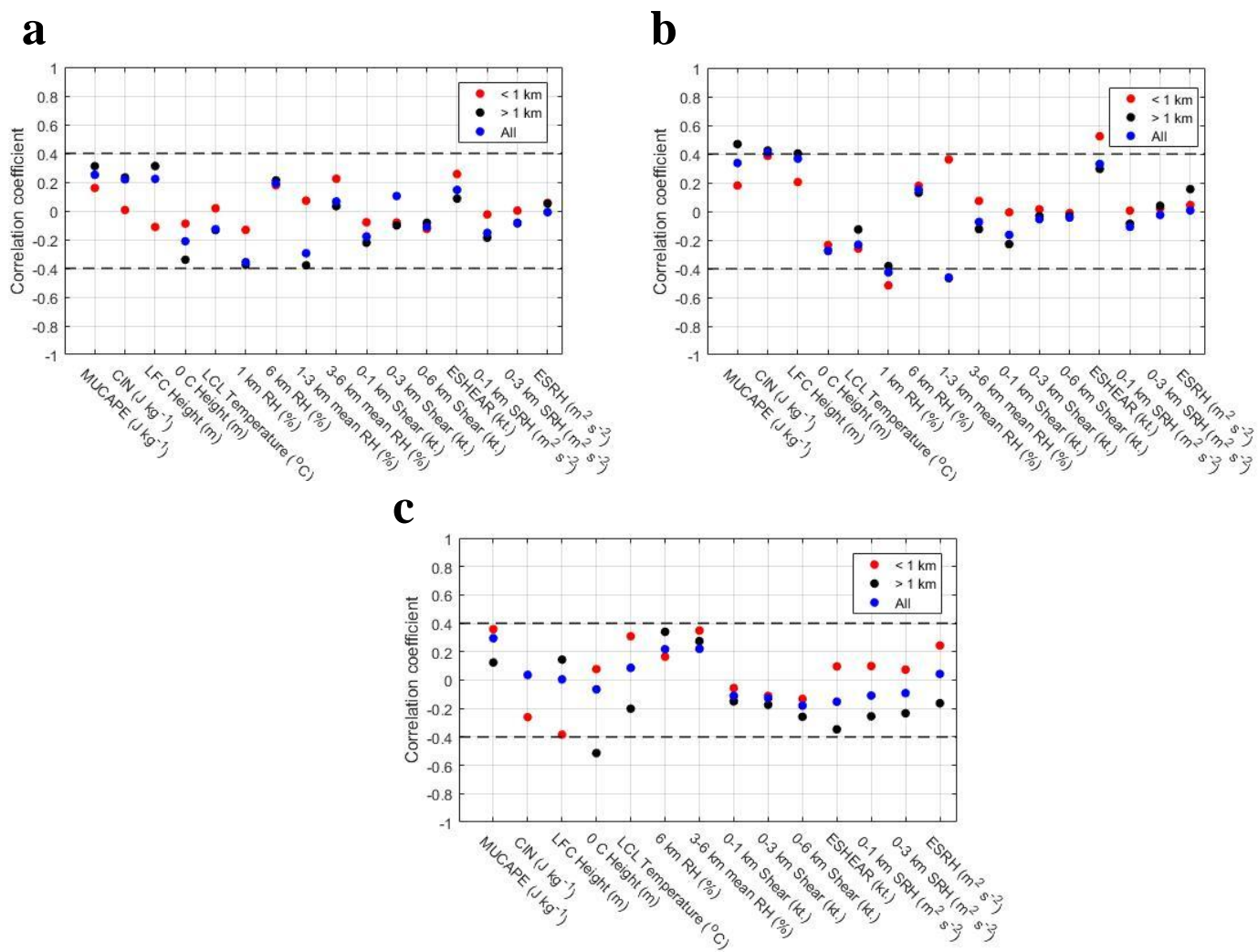


Fig. 5.2: Correlation coefficient values calculated for mean HAE (km²) vs. selected environmental variables for a) all environments, b) tornadic environments, and c) nontornadic environments. Storms with HRSV less than 1 km are represented by red dots, storms with a HRSV greater than 1 km by black dots, and all storms combined by blue dots. Dashed lines indicate correlation coefficients with a magnitude of 0.4.

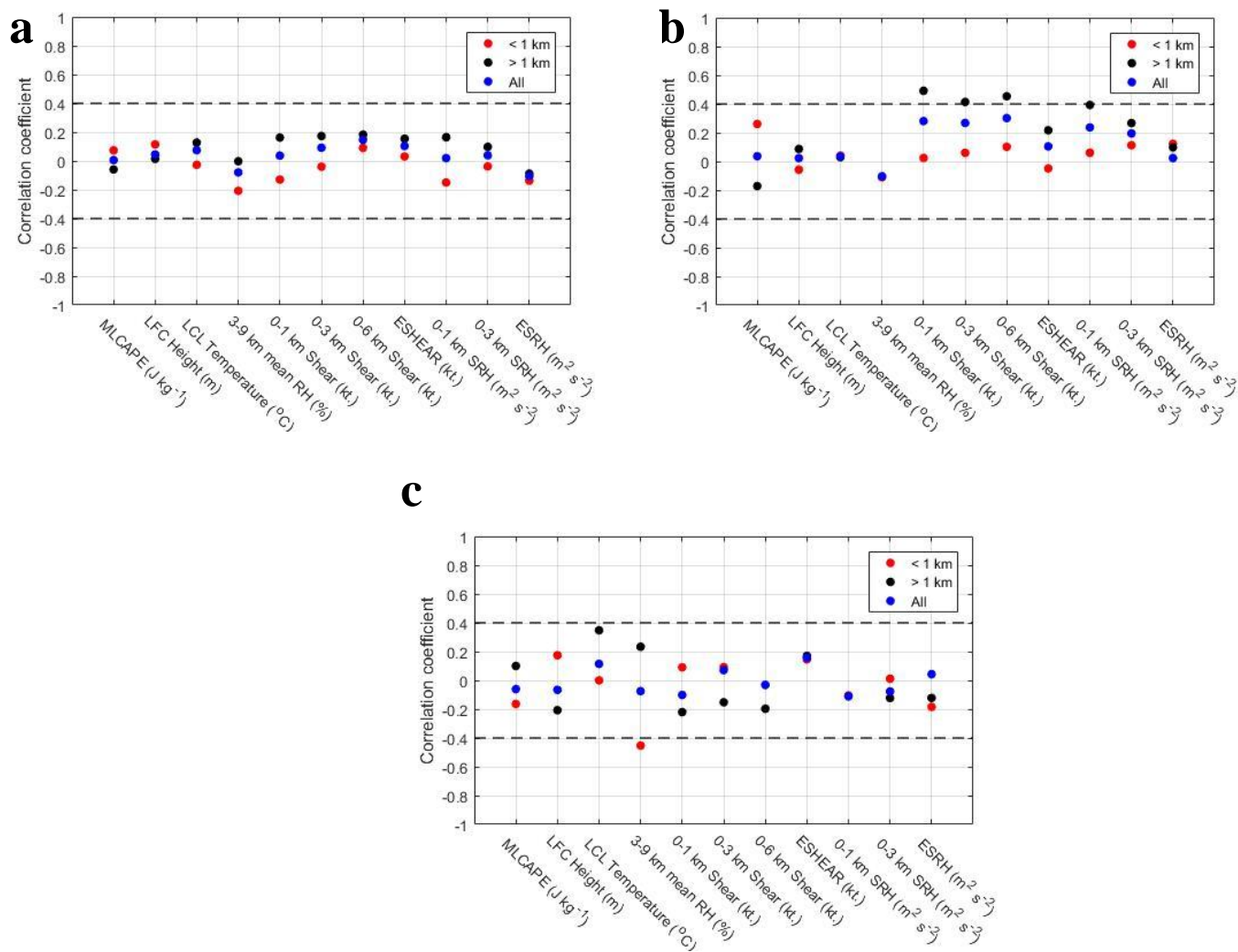


Fig. 5.3: Correlation coefficient values calculated for hail variability vs. selected environmental variables for a) all environments, b) tornadic environments, and c) nontornadic environments. Storms with HRSV less than 1 km are represented by red dots, storms with a HRSV greater than 1 km by black dots, and all storms combined by blue dots. Dashed lines indicate correlation coefficients with a magnitude of 0.4.

Table 5.4: Quartile values for mean HAE (km²) and hail variability.

Quartile	Mean Areal Extent	Variability
Minimum	1.92 km ²	0.16
First (25%)	23.63 km ²	0.42
Second (50%)	43.93 km ²	0.55
Third (75%)	77.97 km ²	0.72
Maximum	297.52 km ²	1.31

I. Thermodynamic Parameters

Previous modeling and observational studies have shown that the evolution of storm characteristics is highly associated with upon various thermodynamic parameters such as CAPE; LFC, LCL, freezing level heights; and LFC and LCL temperatures (e.g., Weisman and Klemp 1982; McCaul and Weisman 2001; Kirkpatrick et al. 2007, 2009, 2011). Model simulations have shown that properties of thermodynamic profiles are correlated to an increase in updraft strength, which in turn can lead to an increase in hydrometeor production (Gilmore et al. 2004). These properties include variables such as CAPE, LFC height, and cloud-base temperature (Kirkpatrick et al. 2007, 2009, 2011).

MLCAPE

Previous studies suggest a relationship between CAPE and updraft characteristics such as updraft strength (Weisman and Klemp 1982; Kirkpatrick et al. 2007; James and Markowski 2010; Naylor and Gilmore 2014). Observational studies such as Van Den Broeke (2016) have also shown that hail variability is directly proportional to the environmental MLCAPE value. No correlations of substantial magnitude are found when inspecting all storms, nontornadic storms, or tornadic storms in the dataset, even when taking HRSV into consideration. Neither LOW MLCAPE nor HIGH MLCAPE environments produced statistically different HAE for all six categories examined, using a Wilcoxon-Mann-Whitney p -test. However, analysis of nontornadic storms with a mean HRSV greater than 1 km show that LOW MLCAPE environments produce a mean variability of 0.393 whereas MID and HIGH MLCAPE environments produce a mean variability of 0.606, which is a statistically significant difference ($p = 0.08$). Tornadic storms with a mean HRSV less than 1 km in environments characterized by HIGH MLCAPE produce a mean variability of 0.499, whereas storms in all other MLCAPE environments produce a mean variability of 0.567; this difference is statistically significant ($p = 0.03$).

MUCAPE

Hail production was hypothesized to increase with an increase in most unstable CAPE (MUCAPE), as modeling studies have shown that the CAPE value is directly

related to updraft strength. A theoretical estimate of the peak updraft vertical velocity can be directly related to CAPE by

$$w_{max} = (2 \cdot CAPE)^{0.5} \quad (9)$$

although this does not take into account mass loading due to condensate, entrainment of ambient air, or pressure perturbation effects. More hail is expected to be present with greater updraft speeds, as an increase in hydrometeor production is expected with an increase in updraft speed (e.g., Rasmussen and Straka 1998; Gilmore et al. 2004; Van Den Broeke 2014).

When tornadic and nontornadic storms were not differentiated, only storms with HRSV over 1 km show moderate correlation between mean HAE and MUCAPE ($r = 0.311$). When mean HAE and MUCAPE are compared in nontornadic storms, storms containing a mean HRSV less than 1 km in height have the strongest correlated ($r = 0.358$). However, MUCAPE differentiates between LOW and HIGH environments for all storms with a HRSV less than 1 km and storms with a HRSV greater than 1 km ($p = 0.07$ and 0.09 , respectively). Storms with a mean HRSV less than 1 km in LOW MUCAPE environments produce a HAE of $\sim 30 \text{ km}^2$ whereas HIGH MUCAPE environments produce HAE of $\sim 56 \text{ km}^2$. Storms with a mean HRSV greater than 1 km in LOW MUCAPE environments produce a HAE of $\sim 71 \text{ km}^2$ whereas HIGH MUCAPE environments produced HAE of $\sim 109 \text{ km}^2$. HIGH MUCAPE environments are statistically different than the combination of LOW and MID environments when considering all storms with mean HRSV greater than 1 km ($p = 0.07$), whereas LOW MUCAPE environments are statistically different than the combination of MID and

HIGH environments when the mean HRSV is less than 1 km ($p = 0.03$). These findings are consistent with theoretical expectations: it is theorized that the MUCAPE values are associated with higher updraft speeds (e.g., Brooks and Wilhelmson 1993; Kirkpatrick 2009), and previous work has shown that higher updraft speeds can be associated with higher hail mixing ratio (e.g., Gilmore et al. 2004; Van Den Broeke 2014).

Mean HAE in tornadic storms with a mean HRSV above 1 km have a moderate correlation with MUCAPE ($r = 0.469$), while all tornadic storms and tornadic storms with a HRSV less than 1 km have weaker positive correlations ($r = 0.337$ and 0.180 , respectively; Fig. 5.4). Even though there is a moderate correlation between HAE and MUCAPE in tornadic storms over 1 km, no statistically significant differences between environments are present for tornadic storms. It is possible that the positive relationship between HAE and MUCAPE is due to the resulting stronger updrafts, which in turn influences overall hydrometeor production as suggested by previous research (e.g., Rasmussen and Straka 1998; Gilmore et al. 2004; Van Den Broeke 2014).

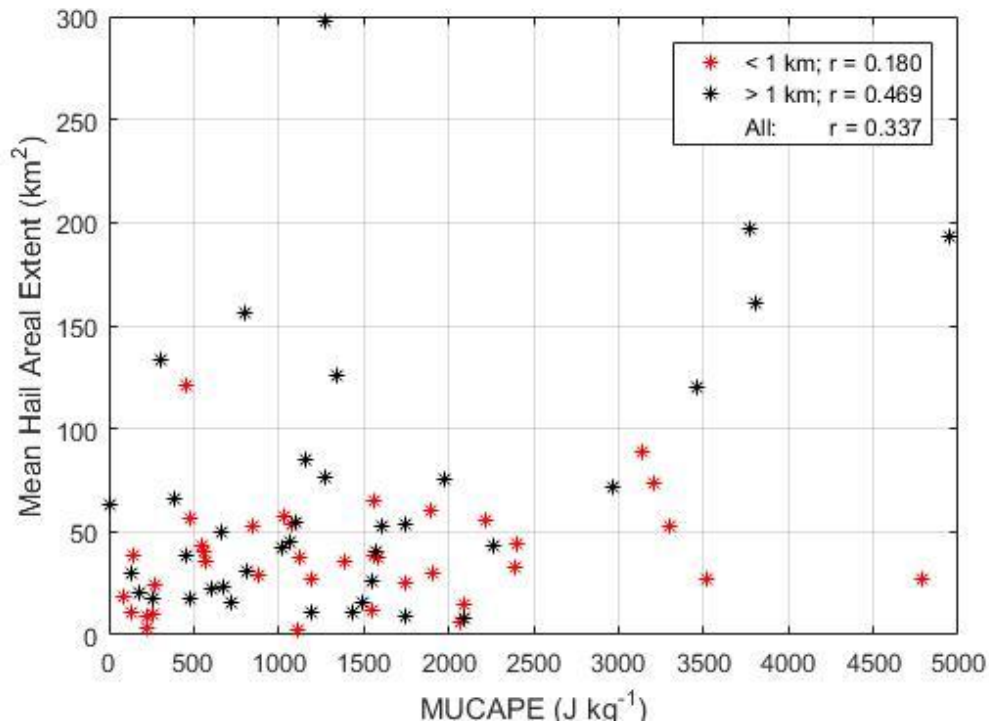


Fig. 5.4: Scatter plot for mean HAE (km²) vs. MUCAPE (J kg⁻¹) for tornadic storms.

Correlation coefficients for storms whose mean HRSV is under 1 km (red stars), storms whose HRSV is over 1 km (black stars), and all storms are listed.

CIN

In the model developed by Van Den Broeke (2016) through multiple linear regression used to predict mean base-scan HAE (Eq. 4), one of the variables included is CIN (J kg⁻¹). Even though this equation, which also includes LFC height (m) and 6-km relative humidity (%) could only explain 51.2% of the HAE variability, the relationship between CIN and mean inferred HAE was further examined in this study. Other

observational studies show that CIN can be predictive of convection including hailstorms (Foote and Wade 1982; Colby 1984).

HAE in both nontornadic storms with a HRSV greater than 1 km and all nontornadic storms is uncorrelated to this environmental variable, whereas nontornadic storms with a HRSV less than 1 km have a slightly stronger negative correlation ($r = -0.261$). The mean HAE of all storms with a HRSV less than 1 km is uncorrelated to CIN, while all storms with a HRSV over 1 km in height and all storms analyzed have slightly higher positive correlations ($r = 0.232$ and 0.219 , respectively) between HAE and CIN. Different CIN environments are not associated with significantly different HAE inferred at the base level scan for nontornadic storms or all storms whose HRSV was below 1 km. However, in all storms with a HRSV above 1 km, there is a significant difference when comparing LOW CIN environments to HIGH CIN environments ($p = 0.05$); storms in LOW CIN environments have an average HAE of $\sim 55 \text{ km}^2$ while storms in HIGH CIN environments have an average HAE of $\sim 105 \text{ km}^2$. Additionally, LOW CIN environments show distinctive HAE signatures when compared to all other environments ($p = 0.07$, respectively).

Examining tornadic storms, however, give a different result (Fig. 5.5). Overall, tornadic storms have a moderate positive correlation to CIN with an r value equal to 0.410. Tornadic storms with HRSV greater than 1 km also have a moderate positive correlation to this thermodynamic parameter ($r = 0.424$), while storms having a mean HRSV less than 1 km have a positive correlation that was slightly lower in magnitude ($r = 0.387$). Moderate to strong relationships are also seen between HAE and CIN in storms

that exhibit HAE greater than the mean value (Fig. 5.6). Defining environments based on the magnitude of CIN also produces significant results when looking at tornadic storms. In tornadic storms with a HRSV below 1 km, LOW CIN environments produce HAE values of $\sim 25 \text{ km}^2$, while storms in other CIN environments are associated with an average areal extent of $\sim 43 \text{ km}^2$ ($p = 0.04$; Fig. 5.7). In general, this result disagrees with prior work, as Van Den Broeke (2016) showed that there was a negative correlation between HAE and CIN (Eq. 4) using a smaller sample of storms. The positive correlation seen between HAE and CIN may be due to the influence of lowered low-level RH within a layer, as discussed later.

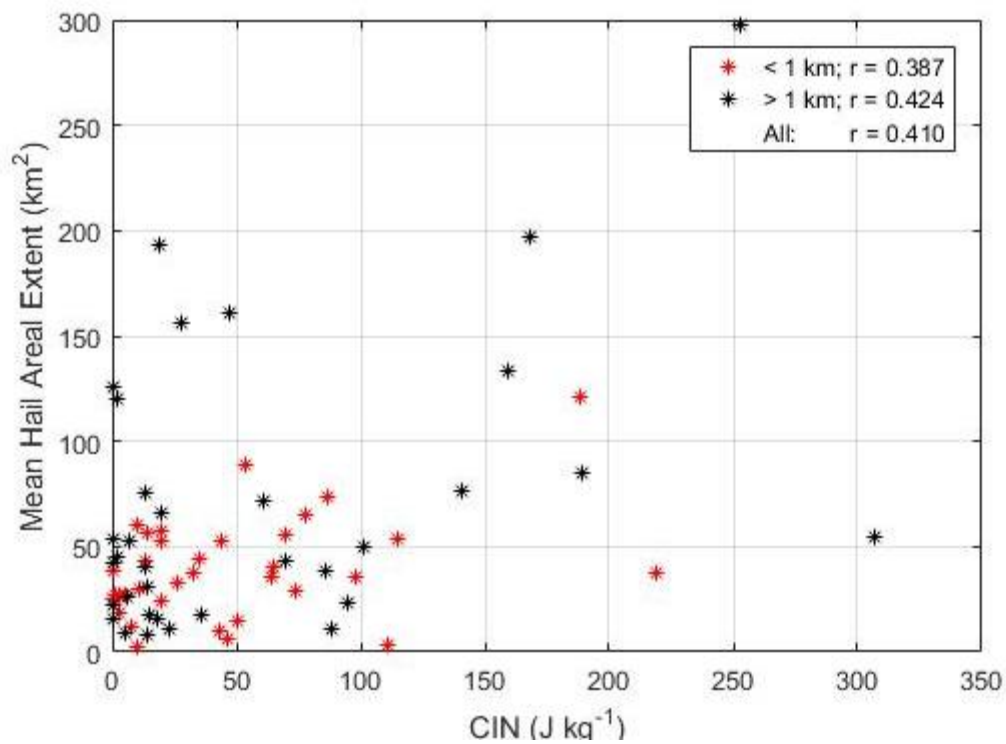


Fig. 5.5: Scatter plot for mean HAE (km^2) vs. CIN (J kg^{-1}) for tornadic storms.

Correlation coefficients for storms whose mean HRSV is under 1 km (red stars), storms whose HRSV is over 1 km (black stars), and all storms are listed.

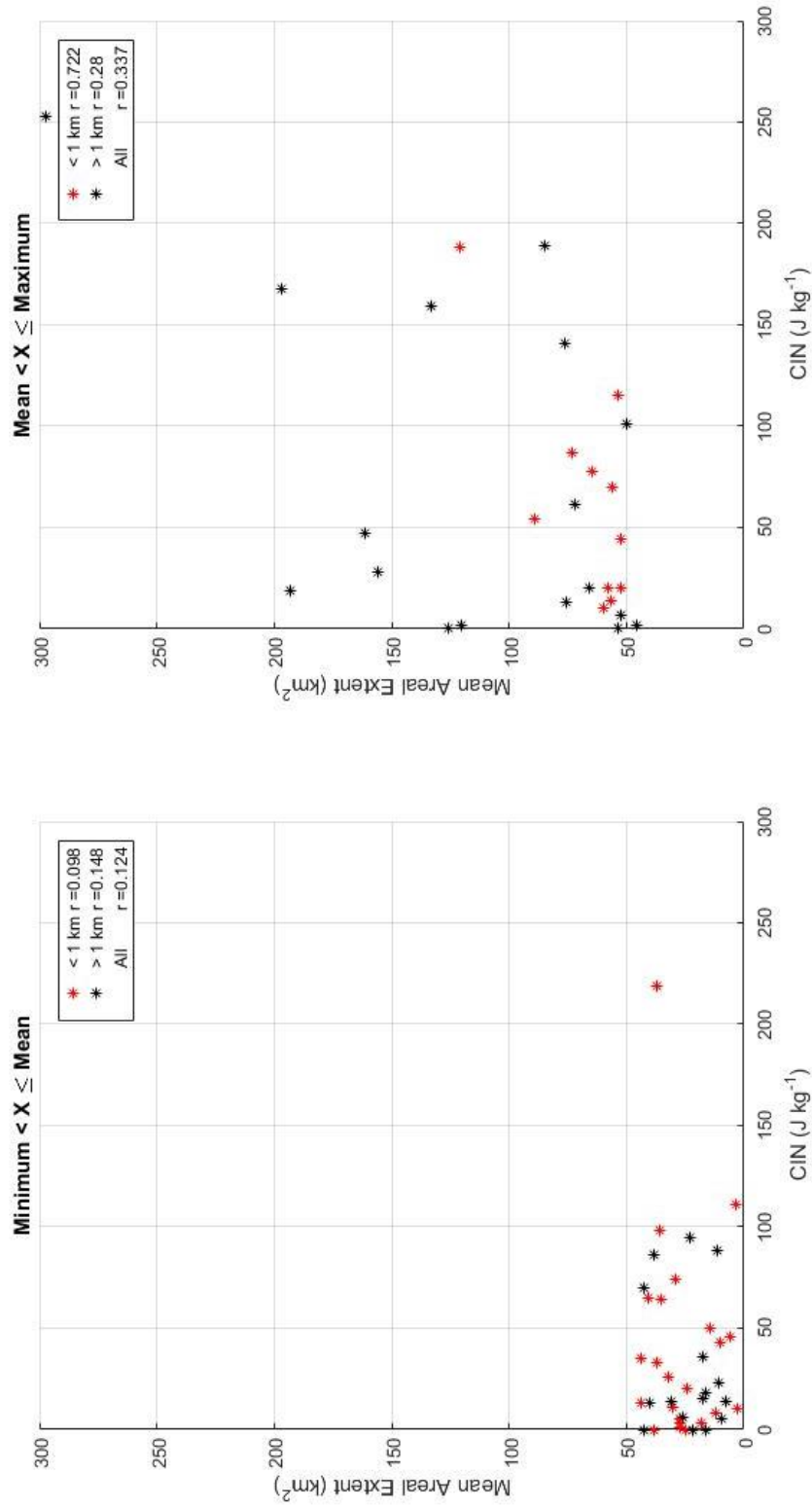


Fig. 5.6: Scatter plots for mean HAE (km²) vs. CIN (J kg⁻¹) for each CIN bin for tornadic storms. Correlation coefficients for storms whose HRSV is under 1 km (red stars), storms that have a HRSV over 1 km (black stars), and all storms are listed for each bin.

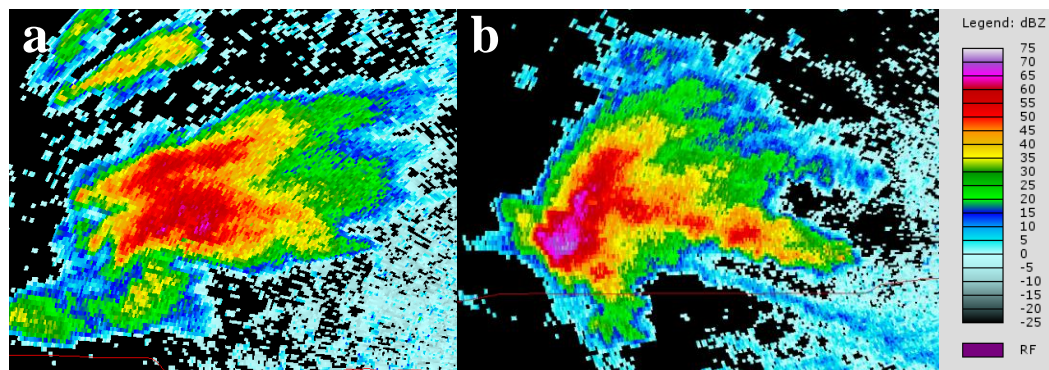


Fig. 5.7: An example of how HAE (km^2) varies in association with CIN. a) Storm in the domain of KINX (Tulsa, Oklahoma) on 20 May 2013 at 2030 UTC; CIN is 1 J kg^{-1} and the mean HAE is 27.30 km^2 . b) Storm in the domain of KGLD (Goodland, Kansas) on 17 June 2013 at 2029 UTC; CIN is 188 J kg^{-1} and the mean HAE is 120.75 km^2 .

LFC Height

Another variable that has been found to have a moderate relationship with mean HAE is the LFC height (Van Den Broeke 2016). A direct relationship between LFC height and mean HAE is hypothesized for a couple reasons. The updraft might be colder on average on days with a high LFC as the updraft will be at a higher altitude. Additionally, there is a fairly strong positive correlation between LFC height and CIN (Table 4.2) that is influenced by low-level RH. A direct relationship is observed when looking at all the storms analyzed in the present study, although the correlation for this dataset was not as strong as the previous study ($r = 0.55$ in Van Den Broeke 2016; $r = 0.22$ in this study).

Storms with a HRSV above 1 km are slightly better correlated ($r = 0.312$) and the storms containing a HRSV below the 1 km threshold are slightly negatively correlated. LOW LFC environments produce an average HAE of $\sim 48 \text{ km}^2$, whereas HIGH LFC environments produce an average HAE of $\sim 126 \text{ km}^2$ when considering all storms with an HRSV above 1 km ($p = 0.006$). Additionally, LOW LFC environments produce statistically different HAE values than other LFC environments, which produce a mean HAE of $\sim 100 \text{ km}^2$ ($p = 0.009$). Mean HAE values found in the HIGH environments are also statistically different than values found in any other environment, although to a lesser degree as LOW and MID environments produce a mean HAE value of $\sim 68 \text{ km}^2$ ($p = 0.02$).

Interrogation of the nontornadic storms showed that storms with a HRSV below 1 km have the strongest correlation, albeit a negative one ($r = -0.384$), whereas the mean HAE in storms above 1 km in height and all nontornadic storms have a slightly positive correlation. There is no relationship between all nontornadic storms and LFC height. Tornadic storms follow this same trend (Fig. 5.8), with both the mean HAE of storms with a mean HRSV above 1 km and all tornadic storms having moderate correlations ($r = 0.403$ and 0.368 , respectively); meanwhile, tornadic storms with HRSV below 1 km have slightly weaker correlation between mean HAE and LFC height. Storms containing mean HAE below the mean value show slight correlation to LFC height, whereas when the HAE of the storm was above the dataset mean value, a moderate relationship is seen (Fig. 5.9). This is especially true when looking at all tornadic storms containing a mean HAE greater than the mean value and tornadic storms with a HRSV less than 1 km ($r =$

0.608). Here as well, when considering values analyzed in tornadic environments with HRSV greater than 1 km, values are different when looking at HIGH and LOW LFC environments. Wilcoxon-Mann-Whitney test p -values show that extreme HIGH and LOW LFC heights were distinguished by mean HAE, as LOW LFC environments are associated with a mean HAE of $\sim 39 \text{ km}^2$ and HIGH LFC environments are associated with a mean HAE of $\sim 119 \text{ km}^2$ ($p = 0.01$; Fig. 5.10). Not only are LOW LFC environments also significantly different than all other environments, which have a mean HAE of $\sim 87 \text{ km}^2$ ($p = 0.02$), but HIGH LFC environments are significantly different than all other environments (mean HAE $\sim 50 \text{ km}^2$; $p = 0.02$). These results generally support those found by Van Den Broeke (2016); as the LFC height increased, it was generally closer to the 0°C level (and therefore colder), although there was almost no correlation between these two variables (Table 4.2).

LFC height appeared to exhibit a strong negative relationship to hail variability in previous research (Van Den Broeke 2016), so this relationship was investigated more in depth. The highest-magnitude correlation between hail variability and LFC height is in nontornadic storms containing a HRSV greater than 1 km in height ($r = -0.207$). This value is negative as found in previous research, although a few of the other data subsets had positive correlations (e.g., variability in nontornadic storms with a HRSV less than 1 km). HIGH LFCs for nontornadic storms with a HRSV above 1 km have statistically less variable HAE (0.53) whereas LFC heights lower than 2625 m have more variable HAE (0.63) ($p = 0.07$).

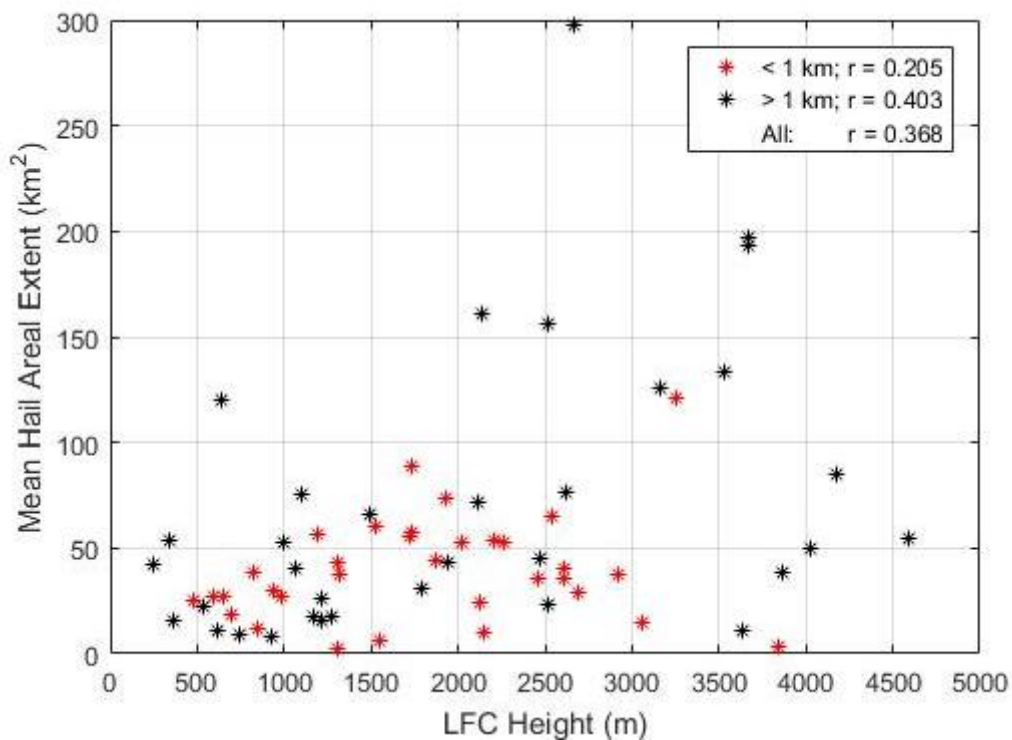


Fig. 5.8: Scatter plot for mean HAE (km²) vs. LFC height (m) for tornadic storms.

Correlation coefficients for storms whose mean HRSV is under 1 km (red stars), storms whose HRSV is over 1 km (black stars), and all storms are listed.

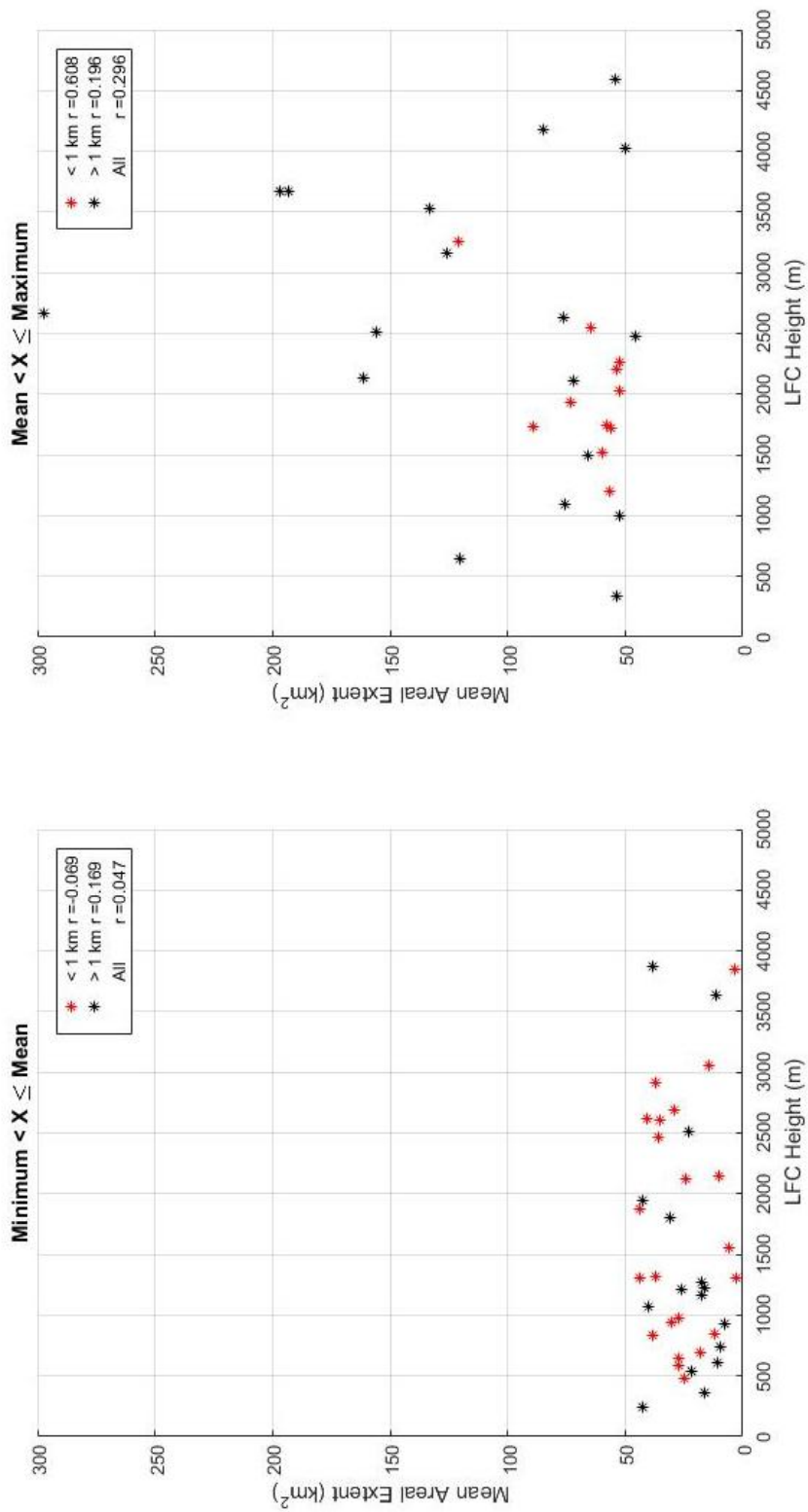


Fig. 5.9: Scatter plots for mean HAE (km²) vs. LFC height (m) for each LFC height bin for tornadic storms. Correlation coefficients for storms whose HRSV is under 1 km (red stars), storms that have a HRSV over 1 km (black stars), and all storms are listed for each bin.

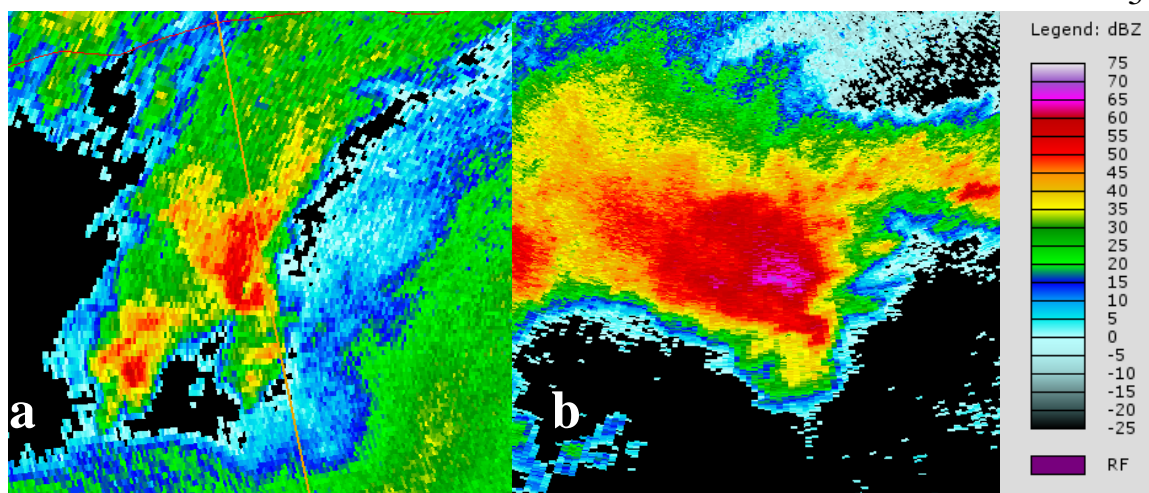


Fig. 5.10: An example of how HAE (km^2) varies in association with LFC height. a) Storm in the domain of KFFC (Atlanta, Georgia) on 18 August 2013 at 2334 UTC; LFC height is 743 m and the mean HAE is 9.44 km^2 . b) Storm in the domain of KABR (Aberdeen, South Dakota) on 21 June 2013 at 1855 UTC; LFC height is 3,666 m and the mean HAE is 196.95 km^2 .

Ambient 0°C Level

The hypothesis that there would be an inverse relationship between the altitude of the 0°C level and the mean inferred HAE was tested. This inverse relationship was hypothesized the understanding that a lower 0°C level would allow onset of melting closer to the surface, resulting in more hail mass surviving to the base-scan level. When studying the relationship between mean inferred HAE of tornadic storms and the environmental freezing level, an inverse relationship is seen in all three tornadic subsets: all tornadic storms, storms with an HRSV below 1 km, and storms with an HRSV above

1 km ($r = -0.274$, -0.235 , and -0.277 respectively). HAE in nontornadic storms containing a HRSV greater than 1 km show an even stronger inverse relationship ($r = -0.514$; Fig. 5.11 and 5.12). There are also moderate negative correlation values when observations are made between the datasets that did not differentiate between tornadic and nontornadic storms. All storms analyzed that had a HRSV above 1 km in height show this relationship ($r = -0.300$).

Environments containing HIGH freezing levels (above 3850 m) are significantly different than other environments for nontornadic storms and tornadic storms with a HRSV greater than 1 km ($p = 0.07$ and 0.02 respectively). For nontornadic storms, HIGH freezing levels are associated with a mean HAE of $\sim 52 \text{ km}^2$, whereas for all other environments are associated with a mean HAE of $\sim 116 \text{ km}^2$; for tornadic storms, HIGH freezing levels are associated with a mean HAE of $\sim 36 \text{ km}^2$, whereas for all other environments are associated with a mean HAE of $\sim 80 \text{ km}^2$. Additionally, results show a significant difference ($p < 0.01$) when looking at all storms with an HRSV greater than 1 km. A significant difference appears in the mean HAE between environments containing HIGH and LOW freezing levels ($p = 0.005$), as $\sim 40 \text{ km}^2$ and $\sim 126 \text{ km}^2$ of mean hailfall are associated respectively. HIGH freezing levels also produce a significant difference in the amount of HAE inferred when compared against mean HAE in other environments ($\sim 97 \text{ km}^2$; $p = 0.0007$).

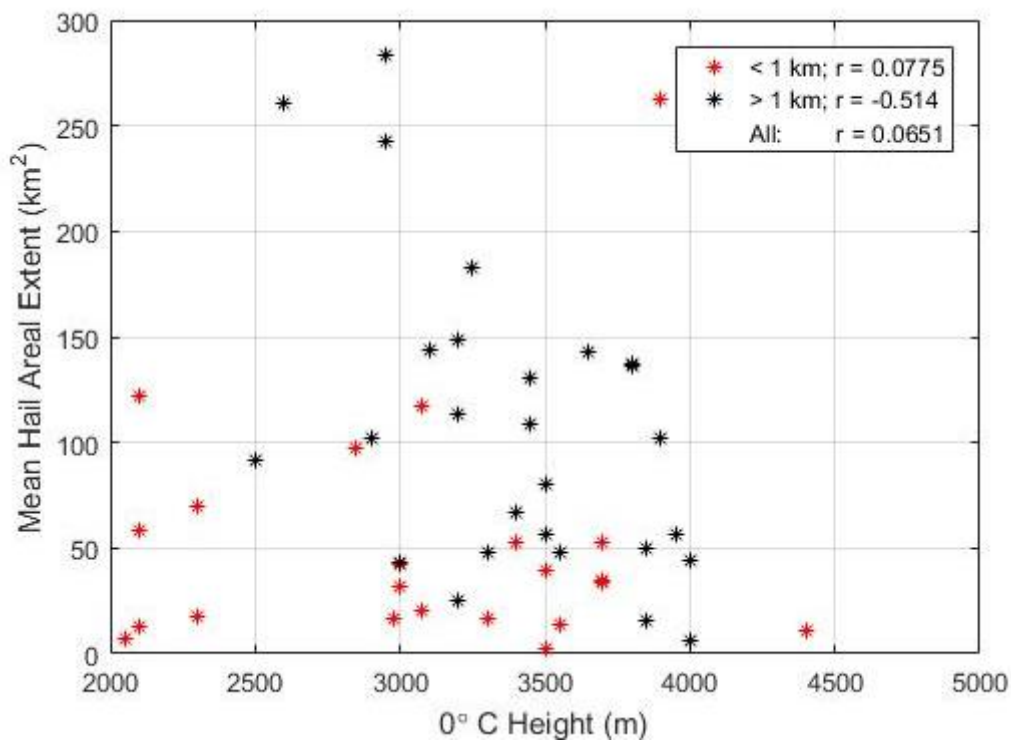


Fig. 5.11: Scatter plot for mean HAE (km²) vs. 0°C height (m) for nontornadic storms. Correlation coefficients for storms whose mean HRSV is under 1 km (red stars), storms whose HRSV is over 1 km (black stars), and all storms are listed.

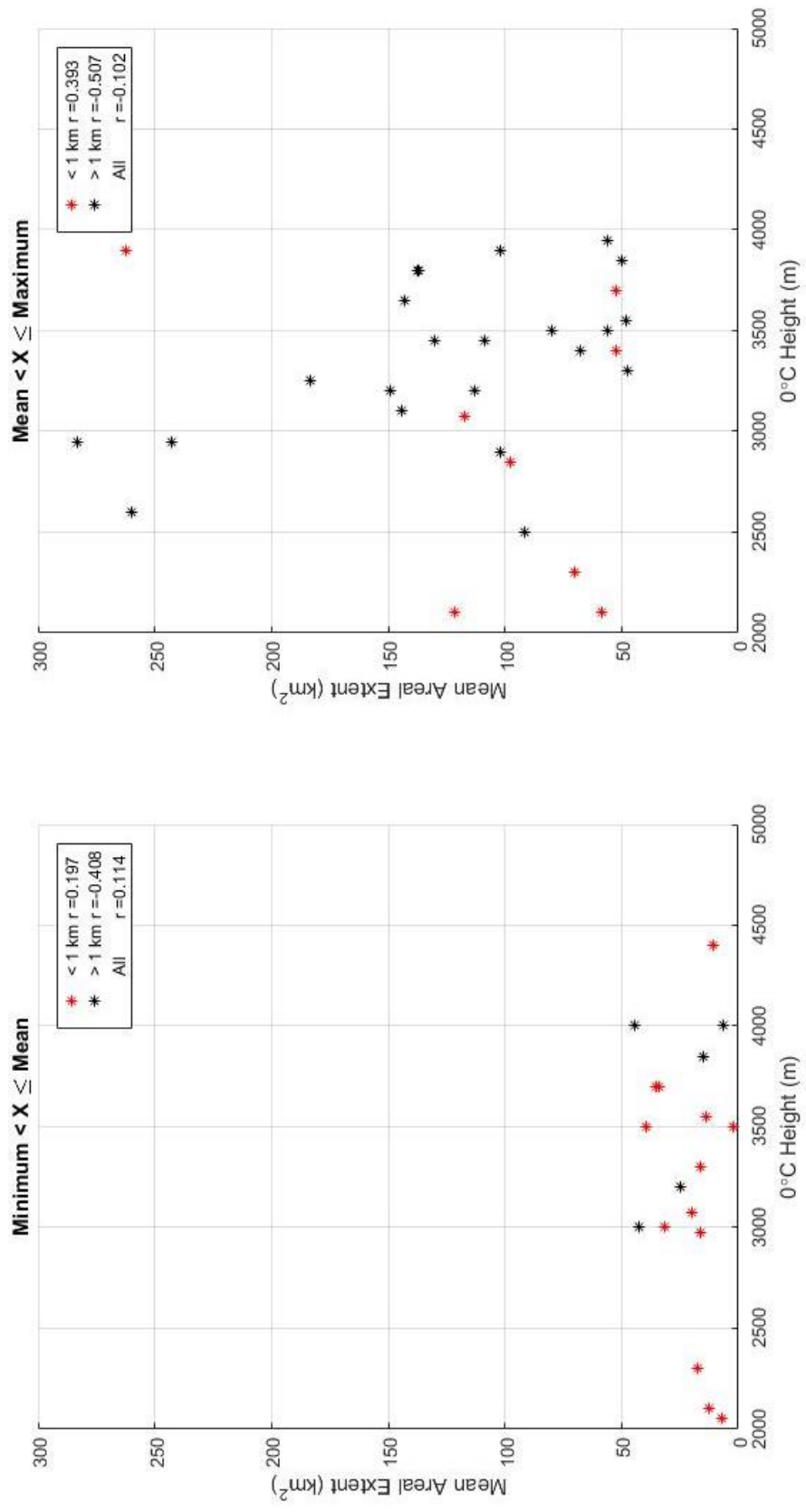


Fig. 5.12: Scatter plots for mean HAE (km²) vs. 0°C height (m) for each 0°C height bin for nontormadic storms. Correlation coefficients for storms whose HRSV is under 1 km (red stars), storms that have a HRSV over 1 km (black stars), and all storms are listed for each bin.

LCL Temperature

Colder mean updrafts, suggested by colder LCL temperatures, are hypothesized to be associated with increased hail production. Colder updrafts would provide more opportunity for hail growth by supercooled water through the riming process. In this dataset, colder LCL temperatures are seen to be associated with higher mean inferred HAE, although there are no strong relationships. When not taking into account the mean HRSV, tornadic storms are the most strongly correlated to LCL temperature ($r = -0.233$). When HRSV was above 1 km, nontornadic storms have an inverse relationship ($r = -0.201$), similar to that found in all tornadic storms.

Studying the relationships between hail variability and LCL temperature did not produce results similar to those shown by previous literature (Van Den Broeke 2016). Surprisingly, almost every subset has no correlation between the hail variability and LCL temperature; nontornadic storms with a HRSV greater than 1 km had the strongest relationship in all the datasets ($r = 0.348$).

b) Moisture Parameters: 1-km RH, 1-3-km mean RH, 3-6-km mean RH, 3-9-km mean RH

Previous observational and modeling studies (e.g., Rasmussen and Heymsfield 1987; Van Den Broeke 2014, 2016) have shown that the moisture characteristics of the layer through which hail descends is important to the amount of hail that reaches the

surface. Drier layers allow greater evaporative cooling when melting begins and thus slow the melting process and allow greater hailstone mass to survive to the surface.

The strongest associations found between inferred HAE and a moisture variable at a single vertical level were with 1-km RH. When examining correlation coefficients between mean HAE and 1-km RH for different subsets of data, moderate relationships are found for all tornadic storms and tornadic storms whose HRSV was below 1 km ($r = -0.425$ and -0.516 respectively, Fig. 5.13). Tornadic storms with HRSV above 1 km also show a slightly weaker negative correlation ($r = -0.381$). Additionally, the mean HAE in nontornadic storms whose HRSV was above 1 km as well as in all storms and all storms with a HRSV greater than 1 km is negatively correlated to 1 km RH, with magnitudes greater than 0.3. A few statistically significant differences are found in mean HAE in environments characterized by different amounts of low-level moisture. The most significant results are seen when looking at all storms with a mean HRSV greater than 1 km. LOW RH environments produce $\sim 134 \text{ km}^2$ in mean HAE, while HIGH RH environments produce a mean HAE of $\sim 61 \text{ km}^2$, which is a significant difference ($p = 0.004$). Additionally, LOW RH environments are significantly different than other environments, which have a mean HAE of $\sim 59 \text{ km}^2$ ($p = 0.0001$).

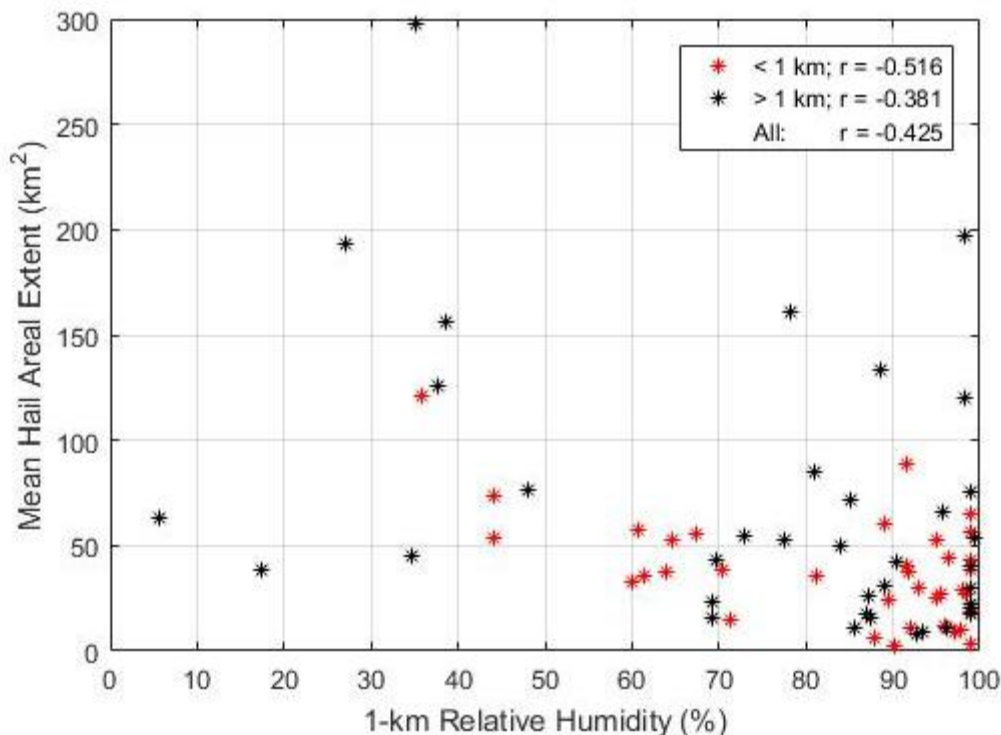


Fig. 5.13: Scatter plot for mean HAE (km²) vs. 1-km RH (%) for tornadic storms.

Correlation coefficients for storms whose mean HRSV is under 1 km (red stars), storms whose HRSV is over 1 km (black stars), and all storms are listed.

The 1-3 km mean RH was calculated as a pressure-weighted value (%) in order to characterize the environment through which hail was descending instead of simply using the value at one height. Similar results to those seen when looking at 1-km RH are observed. All tornadic storms, tornadic storms below 1 km in height, and tornadic storms greater than 1 km in height all show moderate negative relationships ($r = -0.461$, -0.362 , and -0.466 respectively; Fig. 5.14). All storms above 1 km in height and nontornadic

storms below 1 km in height also show moderate relationships between HAE and 1-3 mean RH, although the relationship in nontornadic storms is positive ($r = -0.379$ and 0.392 respectively).

The negative relationships with this environmental variable, as well as those seen with 1 km RH, support the hypothesis that drier layers of the atmosphere tend to produce larger inferred HAEs, most likely due to greater evaporative cooling. A decreased low-level RH in a layer could also help explain the relationships seen between the HAE and CIN or LFC height. A reduction in the low-level RH is one way that the amount of CIN could increase. Enhancement of CIN is one of ways that brings about an increased LFC height and explains the high correlation between these two variables, as seen in Table 4.2.

Significant differences between average HAE are somewhat related to this measure of the dryness of the 1-3 km layer of the atmosphere. Most of those differences occurred when tornadic and nontornadic environments were not discriminated. In all storms with a HRSV greater than 1 km, there is a significant difference in the amount of hailfall in LOW 3-6 km RH environments ($p = 0.002$); storms in environments characterized by LOW 1-3 km RH produce a mean HAE of $\sim 119 \text{ km}^2$, while in all other environments a mean HAE of $\sim 64 \text{ km}^2$ is produced. LOW RH environments are also statistically different than HIGH RH environments, which produce $\sim 44 \text{ km}^2$ of HAE ($p = 0.002$). LOW RH environments are also statistically different when observing tornadic storms with a HRSV greater than 1 km. These environments are distinguished by HAEs of $\sim 103 \text{ km}^2$, whereas HIGH RH environments show HAEs of $\sim 38 \text{ km}^2$ ($p = 0.09$).

Additionally, storms in MID and HIGH environments produce $\sim 53 \text{ km}^2$, which is also statistically different than LOW environments ($p = 0.08$).

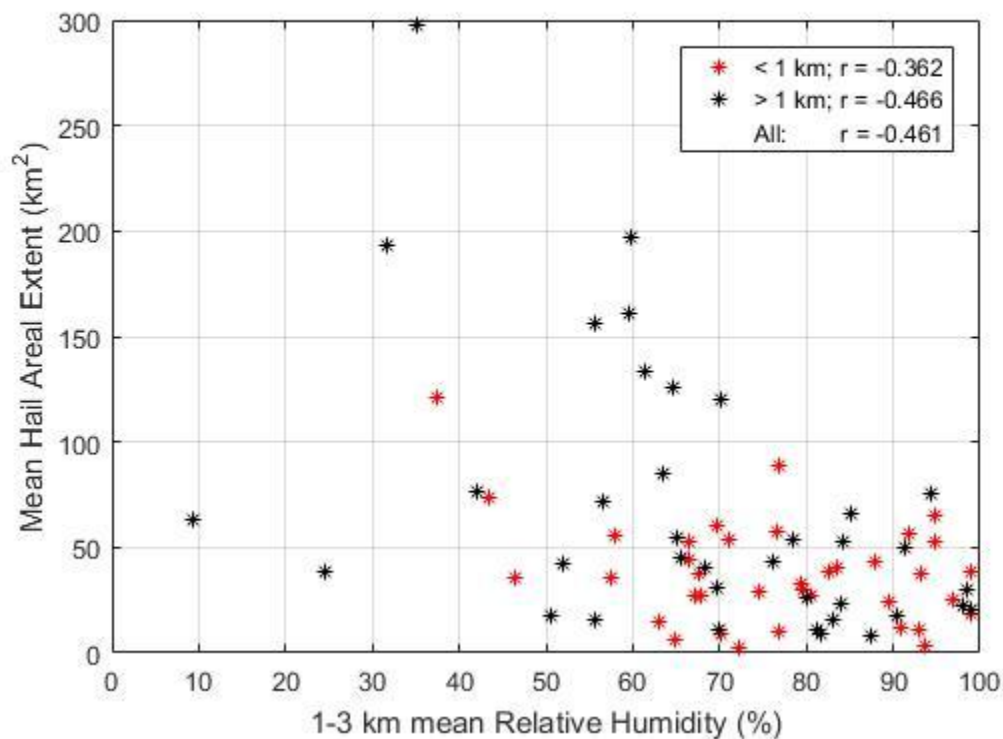


Fig. 5.14: Scatter plot for mean HAE (km²) vs. 1-3-km RH (%) for tornadic storms.

Correlation coefficients for storms whose mean HRSV is under 1 km (red stars), storms whose HRSV is over 1 km (black stars), and all storms are listed.

The 3-6 km mean RH was also calculated; correlation magnitudes between 3-6 km mean RH and mean HAE are greater than 0.2 for all nontornadic storms, nontornadic storms with a HRSV greater than 1 km, and nontornadic storms with a HRSV less than 1

km ($r = 0.220, 0.349, \text{ and } 0.275$ respectively; Fig. 5.15). When the results are separated by the mean value (Fig. 5.16), there is a relatively high correlation between HAE and 3-6 mean RH in the upper half of the storms that had an HRSV less than 1 km ($r = 0.585$) as well as a moderate relationship when observing all nontornadic storms in the upper half of the data sub-set and nontornadic storms with a HRSV greater than 1 km ($r = 0.341$ and 0.319 respectively).

Significant differences between average HAE are somewhat related to this measure of the dryness of this particular layer of the atmosphere. Most of those differences occurred when tornadic and nontornadic environments were not discriminated. In all storms with a HRSV less than 1 km, there is a significant difference in the amount of hailfall in LOW 3-6 km RH environments ($p = 0.09$); in storms with LOW 3-6 km RH, a mean HAE of $\sim 29 \text{ km}^2$ is observed, while in all other environments a mean HAE of $\sim 47 \text{ km}^2$ is observed. Meanwhile in all storms that had a HRSV greater than 1 km, HIGH 3-6 km RH environments are associated with a mean HAE of $\sim 68 \text{ km}^2$, whereas all other environments are associated with an average HAE $\sim 88 \text{ km}^2$, a significant difference ($p = 0.05$). When tornadic storms whose HRSV was greater than 1 km are analyzed, it is observed that environments containing high values of 3-6 km mean RH produce a mean HAE of $\sim 29 \text{ km}^2$, while all other environments produce a mean HAE of $\sim 83 \text{ km}^2$, which is also a significant difference ($p = 0.01$).

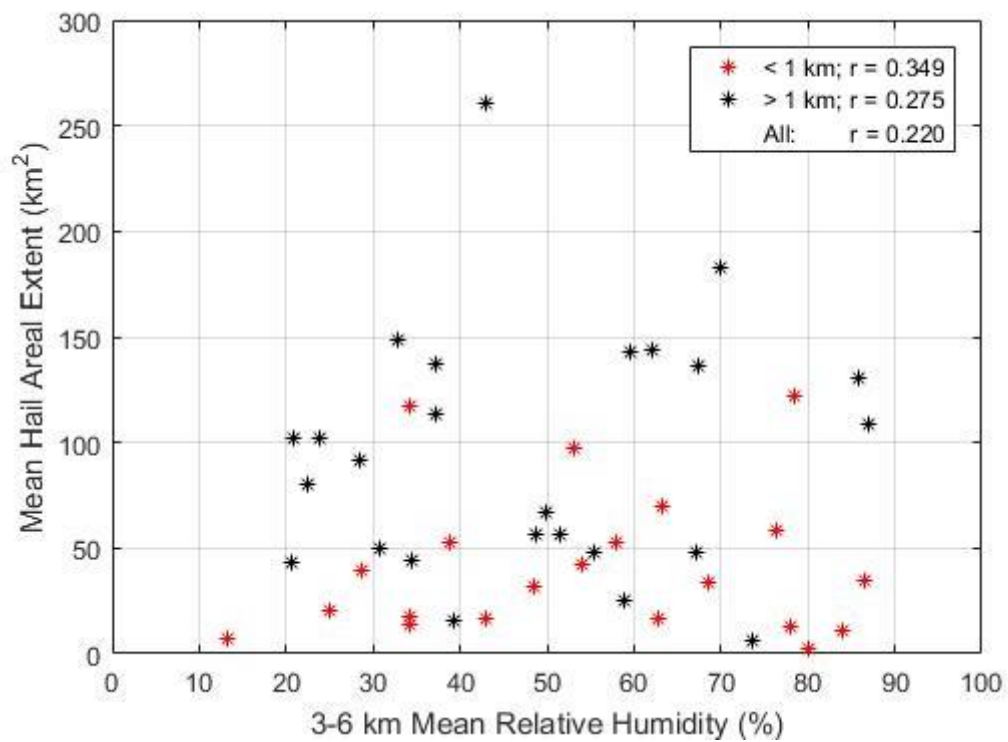


Fig. 5.15: Scatter plot for mean HAE (km²) vs. 3-6-km RH (%) for nontornadic storms. Correlation coefficients for storms whose mean HRSV is under 1 km (red stars), storms whose HRSV is over 1 km (black stars), and all storms are listed.

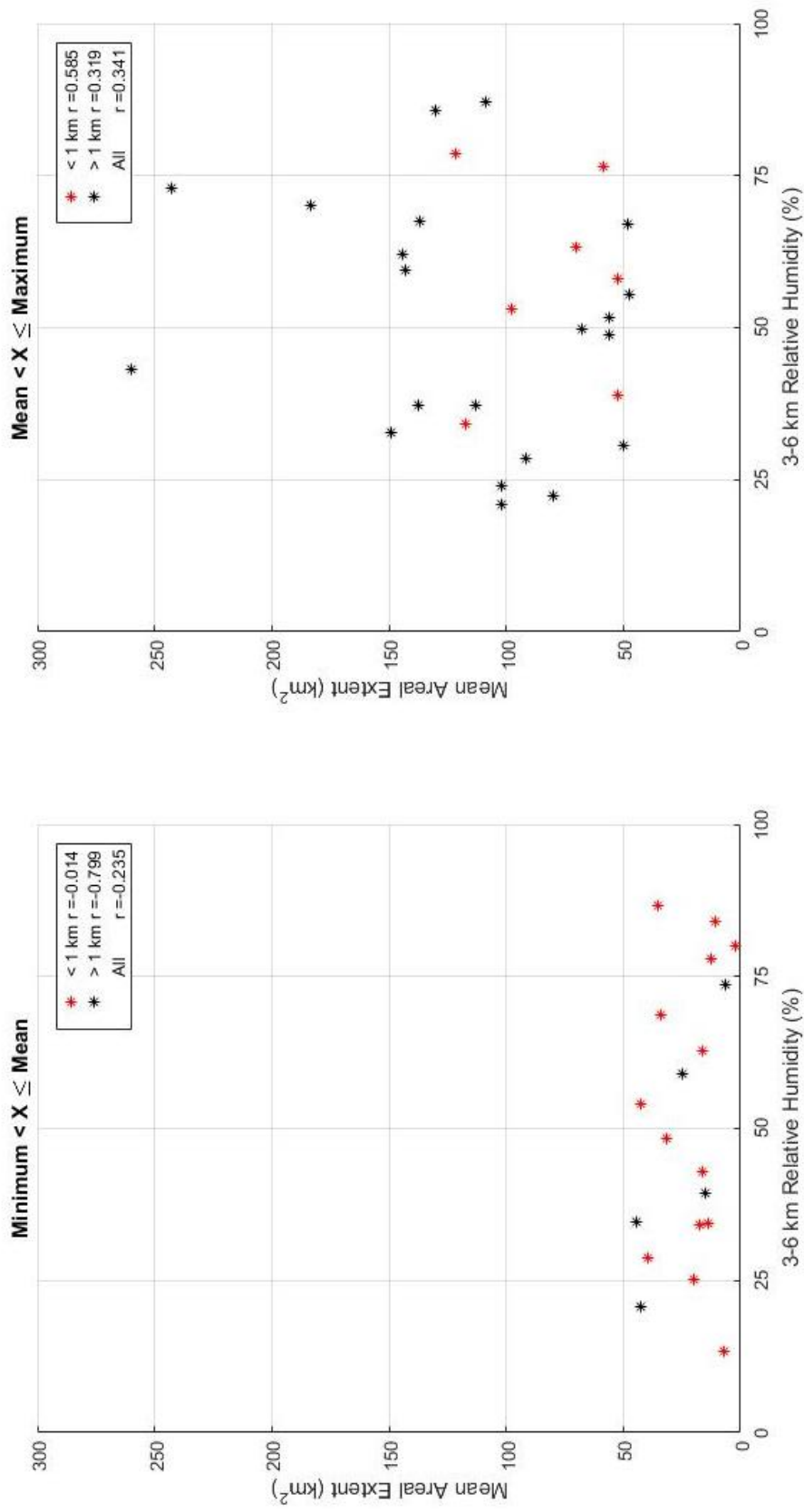


Fig. 5.16: Scatter plots for mean HAE (km²) vs. 3-6 km RH (%) for each RH bin for nontornadic storms. Correlation coefficients for storms whose HRSV is under 1 km (red stars), storms that have a HRSV over 1 km (black stars), and all storms are listed for each bin.

The previous observational study by Van Den Broeke (2016), which utilized a much smaller dataset, showed that the variability of inferred HAE decreased with increasing mean RH in the 3-9 km layer ($r = -0.48$); the previous study did not speculate as to why these variables were associated in this way. The hail variability of both nontornadic storms and all storms with a HRSV less than 1 km exhibits the same inverse relationship ($r = -0.453$ and -0.207 respectively, Fig. 5.17). Contrastingly, though, hail variability in nontornadic storms with a HRSV greater than 1 km in the upper half of all hail variability values has a moderate positive correlation with 3-9 km mean RH ($r = 0.491$; Fig. 5.18). Throughout the subsets of data studied, the variability in storms with low percentages of 3-9 km mean RH is not significantly different than the variability in storms with high percentages of this moisture parameter. In addition, environments with neither LOW nor HIGH mean 3-9 km RH values are associated with a significantly different amount of variability in HAE through the analysis period.

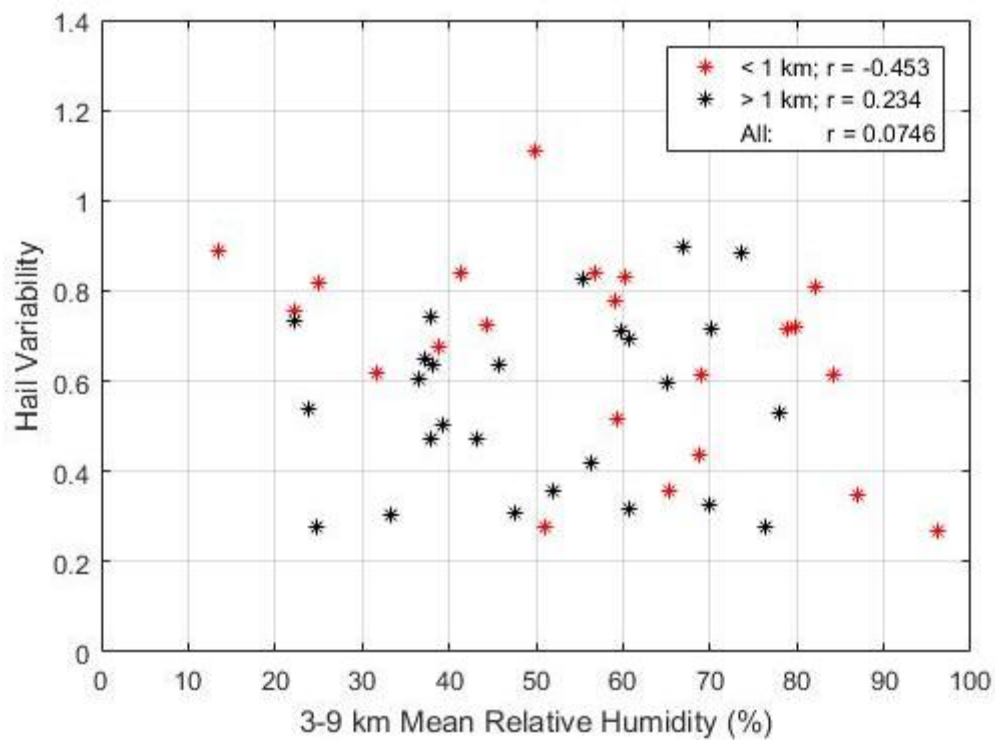


Fig. 5.17: Scatter plot for hail variability vs. 3-9-km RH (%) for nontornadic storms.

Correlation coefficients for storms whose mean HRSV is under 1 km (red stars), storms whose HRSV is over 1 km (black stars), and all storms are listed.

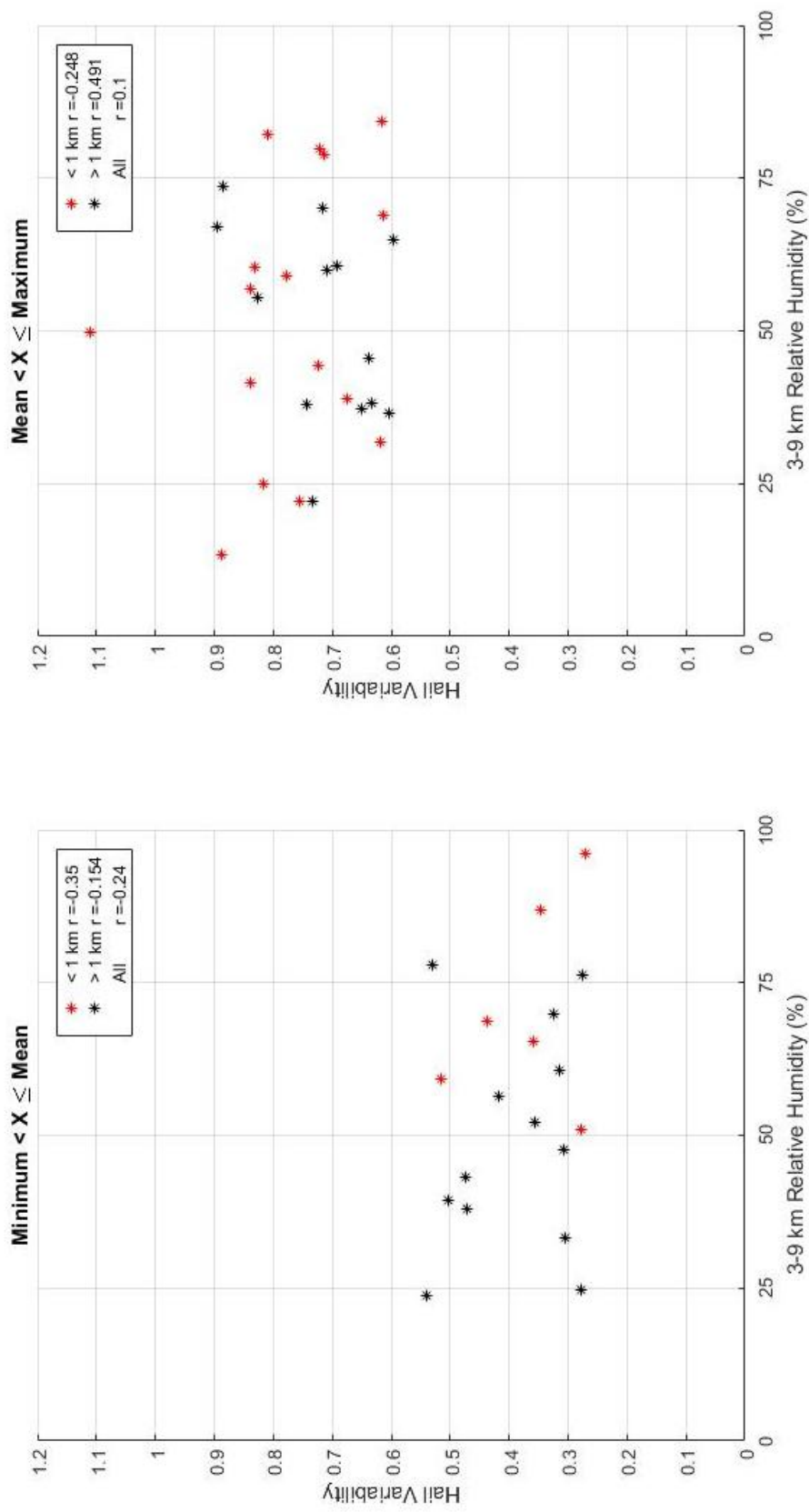


Fig. 5.18: Scatter plots for hail variability vs. 3-9-km RH (%) for each RH bin for nontornadoic storms. Correlation coefficients for storms whose HRSV is under 1 km (red stars), storms that have a HRSV over 1 km (black stars), and all storms are listed for each bin.

c) Shear parameters

Shear parameters, such as bulk shear and storm relative helicity (SRH) through different layers, distinguish storm structure (e.g., multi-cellular vs. supercell; Weisman and Klemp 1982, 1984). Furthermore, these parameters are closely tied to precipitation production through the life cycle of supercells (e.g., Rasmussen and Straka 1998; Gilmore et al. 2004). Prior modeling work (e.g., Van Den Broeke et al. 2010; Dennis and Kumjian 2014) as well as observational studies (e.g., Van Den Broeke 2016) have shown that hail production should have a positive relationship with increases in storm relative winds. Stronger shear values should be associated with a higher mixing ratio of ice-phase particles, including hail (Van Den Broeke et al. 2010). Additionally, an increase in updraft strength due to an increase in shear has been observed in modeling studies (Weisman and Klemp 1984).

0-1-km shear, 0-3-km shear, 0-6-km shear

Analysis of the data subsets show that only a few moderate relationships existed between mean HAE and 0-1 km shear. Both tornadic storms and all storms with an HRSV above 1 km have a negative correlation between HAE and this shear parameter ($r = -0.229$ and -0.222 respectively). Moreover, size of the inferred hail region is not significantly different depending upon the amount of 0-1 km environmental shear. Shear values through a deeper layer (0-6 km) were also analyzed in comparison to mean HAE.

Most of the data subsets analyzed do not show significant correlations between 0-6 km shear values and HAE; although nontornadic storms with HRSV below 1 km have a moderate correlation ($r = -0.258$). Similar results were expected, due to the high correlation between the 0-1 km and 0-6 km shear (Table 4.2). However, HAE is significantly different in LOW and HIGH shear environments. Nontornadic environments with HRSV less than 1 km and LOW values of 0-6 km shear have a HAE of $\sim 65 \text{ km}^2$, while all other environments show a mean HAE of $\sim 49 \text{ km}^2$, which is a significant difference ($p = 0.09$). Based on these results, 0-6 km shear is the best shear variable predictor of mean HAE.

Stronger relationships were seen when comparing hail variability and shear. A moderate relationship is seen between hail variability and 0-1 km shear for all tornadic storms with HRSV $< 1 \text{ km}$ ($r = 0.463$, Fig. 5.19). Significant differences are observed in the variability of mean HAE when looking at 0-1 km shear in tornadic environments when the average HRSV was $\geq 1 \text{ km}$. LOW shear environments produce a mean coefficient of variation of ~ 0.453 , while HIGH shear environments produce a mean coefficient of variation of ~ 0.709 ; this is a significant difference ($p = 0.05$; Fig. 5.20). HIGH shear environments are also significantly different from all other shear environments, as the other environments produce a mean coefficient of variation of ~ 0.486 ($p = 0.04$).

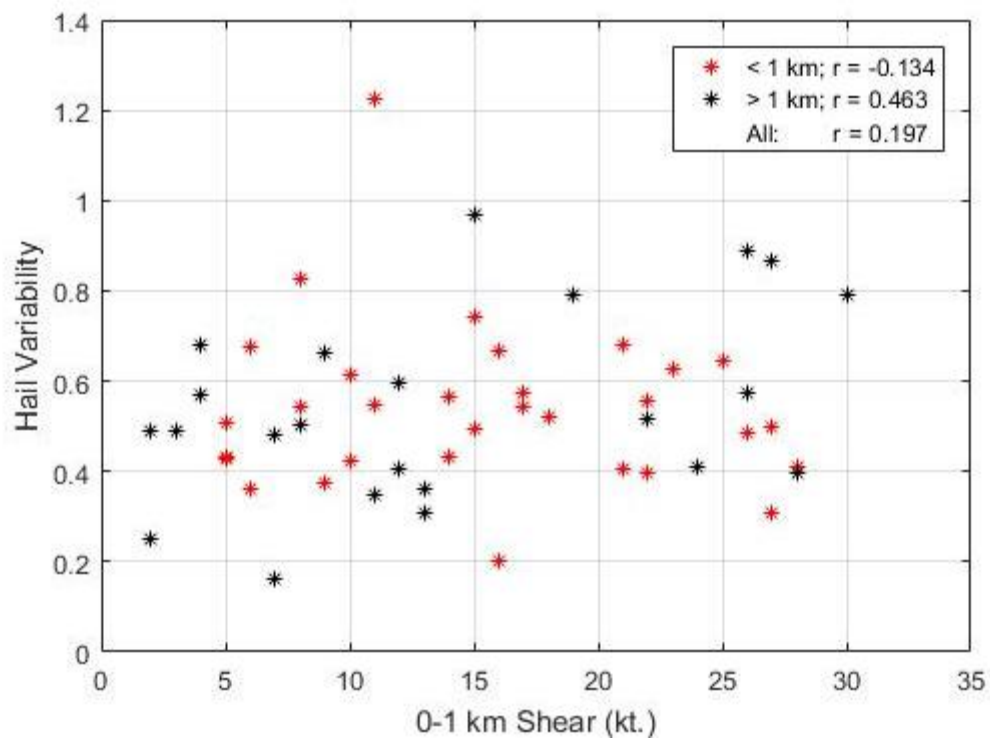


Fig. 5.19: Scatter plot for variability vs. 0-1 km shear (kt.) for tornadic storms.

Correlation coefficients for storms whose mean HRSV is under 1 km (red stars), storms whose HRSV is over 1 km (black stars), and all storms are listed.

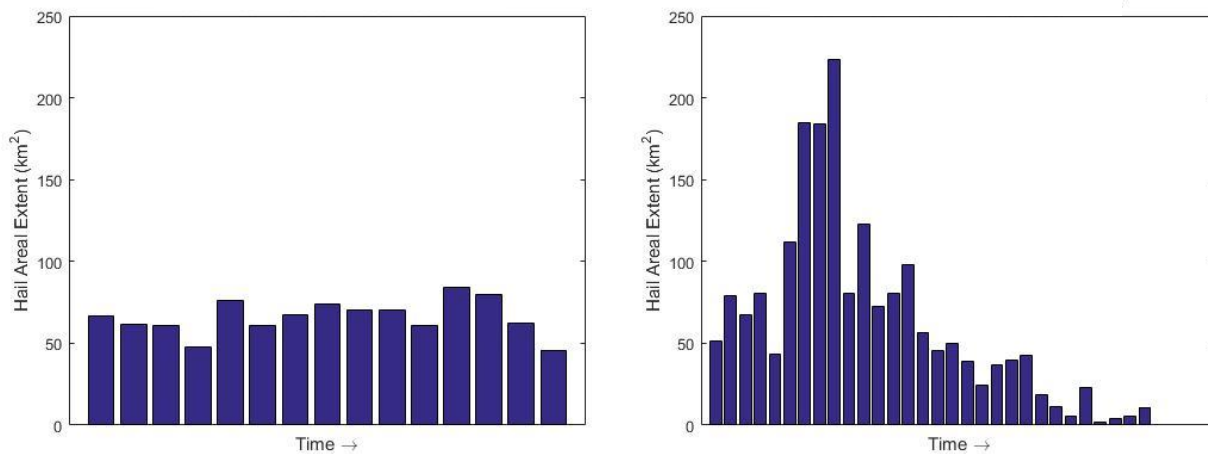


Fig. 5.20: An example of how HAE (km^2) varies cyclically through time as in association with 0-1 km shear. a) A time series of mean HAE from a supercell in the domain of KHPX (Ft. Campbell, Kentucky) from 0000 to 0056 UTC 7 July 2013; variability is ~ 0.16 and shear is 7 kt.; b) a time series of mean HAE from a supercell in the domain of KAMA (Amarillo, Texas) from 2300 UTC 14 August 2013 to 0058 UTC 15 August 2013; variability is ~ 0.8 and shear is 26 kt.

However, tornadic storms with a HRSV greater than 1 km have almost no correlation between mean HAE and 0-3 km and 0-6 km shear. HIGH 0-6 km shear environments are significantly different than other environments in storms greater than 1 km in height ($p = 0.09$) as HIGH shear environments produce a HAE of $\sim 59 \text{ km}^2$, while other environments produce $\sim 100 \text{ km}^2$ of hail. In nontornadic environments with HRSV below 1 km, LOW 0-3 km shear environments produce less variable storms (mean variability of ~ 0.463) while other environments produce storms that have a mean

variability of ~ 0.699 , which is statistically significant ($p = 0.05$). Meanwhile, in tornadic environments with HRSV above 1 km, LOW 0-3 km shear environments (< 19 kt.) produce significantly less variable storms (mean variability ~ 0.454) when compared to HIGH shear environments, which are defined as having shear ≥ 33 kt. (mean variability ~ 0.740 ; $p = 0.03$). Variability in mean HAE is significantly larger in HIGH shear environments than in other shear environments, which have an average variability of ~ 0.499 ($p = 0.04$).

Significant differences in hail variability are also found across differing environments for 0-6 km shear. LOW 0-6 km shear environments for nontornadic environments with HRSV below 1 km contain a mean variability of ~ 0.446 , whereas all other environments contain a mean variability of ~ 0.703 ; this difference is statistically significant ($p = 0.04$). 0-6 km shear also show significant differences in the hail variability in tornadic storms whose HRSV is greater than 1 km. Environments characterized by HIGH values of deep-layer shear have a mean variability of ~ 0.726 , while all other environments have a mean variability of ~ 0.505 , which is a significant distinction ($p = 0.07$). Additionally, environments characterized by HIGH values of 0-6 km shear are significantly different than environments characterized by LOW values of 0-6 shear (mean variability ~ 0.496 ; $p = 0.06$). An example of this difference is seen in Fig. 5.21.

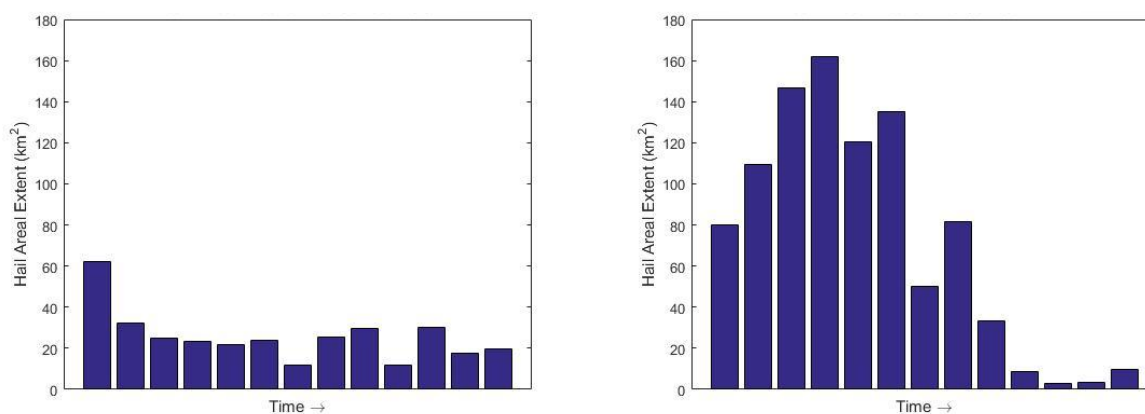


Fig. 5.21: An example of how HAE (km²) varies cyclically through time as a function of 0-6 km shear. a) A time series of mean HAE from a supercell in the domain of KCCX (State College, Pennsylvania) from 1801 to 1856 UTC 27 June 2013; variability is ~ 0.489 and shear is 23 kt.; b) a time series of mean HAE from a supercell in the domain of KTWX (Topeka, Kansas) from 0001 to 0057 UTC 15 April 2012; variability is ~ 0.864 and shear is 76 kt.

These results generally support previous literature (e.g., Gilmore et al. 2004; Van Den Broeke et al. 2010), as an increase in environmental shear produces an increase in mean HAE. Hail production is thought to be tied to mesocyclone cycling and updraft pulses as suggested by Adlerman and Droegemeier (2005) and Van Den Broeke (2010). Adlerman and Droegemeier (2005) showed that an increase in vertical shear magnitude slows down and eventually terminates the cycling process, which would result in less variability in hailfall. However, the results presented here show that hail variability increases with an increase in low-level shear. Part of the disparity may be due to the use

of liquid-only microphysics by Adlerman and Droegemeier (2005). Van Den Broeke (2010) showed the mesocyclone cycling is possible in high-shear environments in simulations with ice-inclusive microphysics. The results presented here show that an increase in shear is associated with increased hail variability. However, taking a look at how hail variability changes over the parameter space (Fig. 5.22), variability remains relatively constant at values of shear greater than 32 kt.

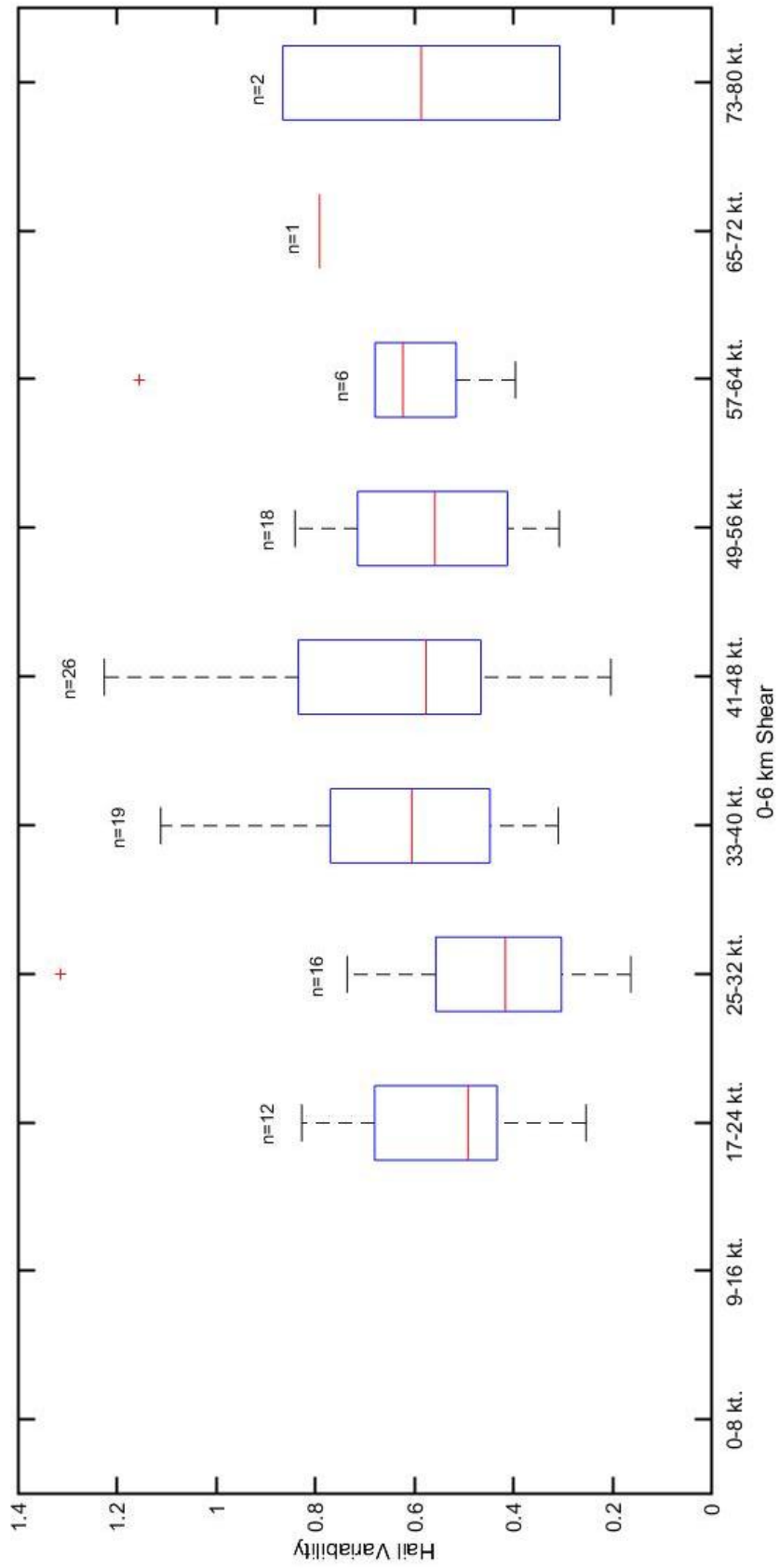


Fig 5.22: Hail variability plotted over shear space. The bottom of each box is the first quartile, and the top of each box is the third quartile. The red bar indicates the median value. Bars are at the 9th and 91st percentiles, with outliers indicated as plus signs.

ESHEAR

To account for shear in the effective inflow layer and account for elevated supercells, the effective bulk shear (ESHEAR) was estimated and relationships were determined between these values and the mean HAE. The effective inflow layer is based on a lifted parcel where the $CAPE \geq 100 \text{ J kg}^{-1}$ and $CIN \geq -250 \text{ J kg}^{-1}$ (Thompson et al. 2007). Initial associations between mean HAE and ESHEAR values are positive, in contrast to the three other shear measurements (0-1 km, 0-3 km, and 0-6 km shear). Even though there is no correlation between all storms (both tornadic and nontornadic) when height is differentiated, an increase in mean HAE with an increase in effective bulk shear is found when all storms are analyzed ($r = 0.146$). All three tornadic storm classifications (all tornadic storms, storms with HRSV below 1 km, and storms with HRSV above 1 km) show relatively moderate relationships between mean areal extent and this shear parameter ($r = 0.331, 0.523, \text{ and } 0.296$ respectively; Fig. 5.23). Additionally, tornadic storms containing mean HAE greater than the mean HAE and an HRSV less than 1 km have a moderate correlation to ESHEAR ($r = 0.558$; Fig. 5.24). HAE in nontornadic storms with a HRSV over 1 km is also correlated to ESHEAR, although this correlation is negative ($r = -0.347$).

Both tornadic storms and all storms with a mean HRSV less than 1 km display low p -values from the Wilcoxon-Mann-Whitney test when the measured variable is mean HAE at the base-level scan. In tornadic storms, LOW ESHEAR environments have statistically lower mean HAE ($\sim 31 \text{ km}^2$) than HIGH ESHEAR environments ($\sim 54 \text{ km}^2$; p

= 0.06). Additionally, there are statistical differences between the mean HAE in HIGH ESHEAR environments versus in all other environments, as a mean value of $\sim 33 \text{ km}^2$ is inferred ($p = 0.04$). However, looking at all storms with a HRSV below 1 km, statistical differences are found between mean HAE in LOW and HIGH ESHEAR environments as mean HAE of $\sim 30 \text{ km}^2$ and $\sim 55 \text{ km}^2$ are inferred ($p = 0.05$). Additionally, a mean HAE of $\sim 53 \text{ km}^2$ is inferred for MID and HIGH ESHEAR environments; this is significantly different than the value produced in LOW ESHEAR environments ($p = 0.07$).

Correlation coefficients between ESHEAR and hail variability were also calculated for each of the data subsets; the hail variability is not correlated to ESHEAR for many of the subsets considered. Tornadic storms with HRSV greater than 1 km have the strongest association between hail variability and ESHEAR ($r = 0.166$). It is deduced, though, that values of HAE variability are not significantly different in environments characterized by different amounts of ESHEAR.

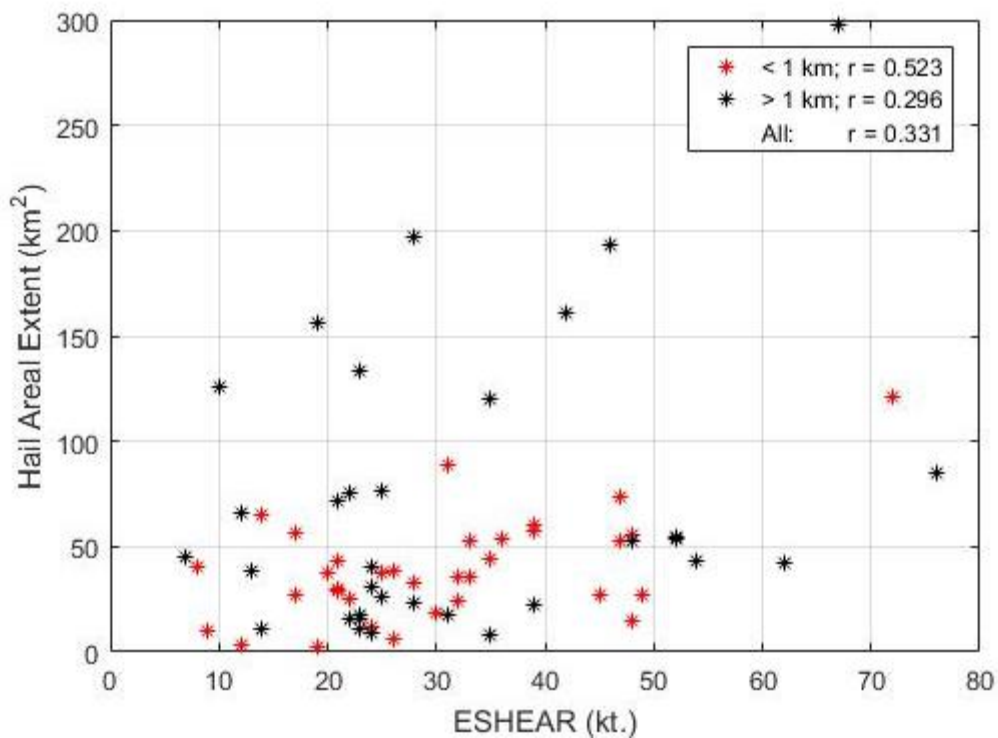


Fig. 5.23: Scatter plot for mean HAE (km^2) vs. ESHEAR (kt.) for tornadic storms.

Correlation coefficients for storms whose mean HRSV is under 1 km (red stars), storms whose HRSV is over 1 km (black stars), and all storms are listed.

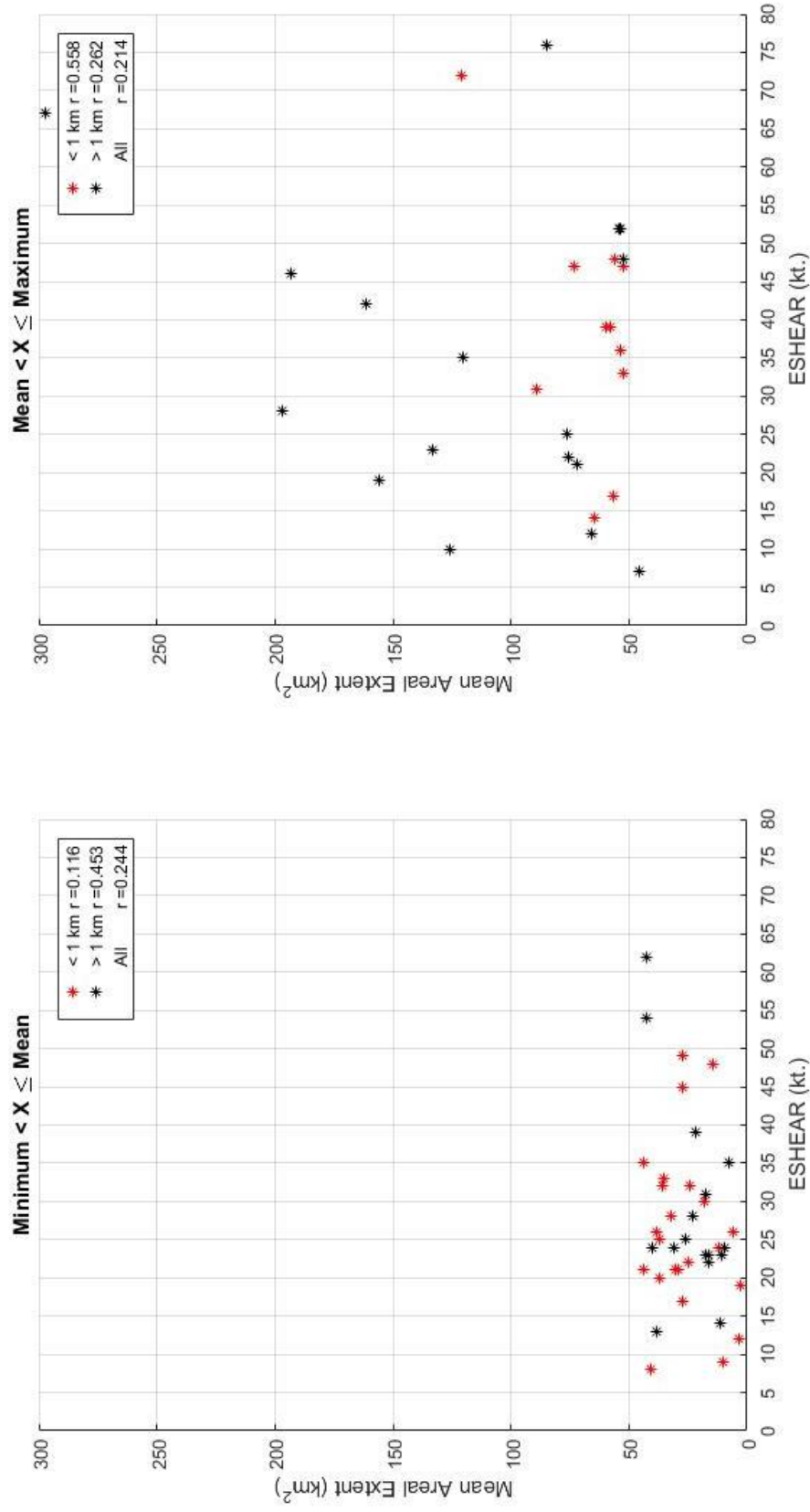


Fig. 5.24: Scatter plots for mean HAE (km²) vs. ESHEAR (kt.) for each ESHEAR bin for tornadic storms. Correlation coefficients for storms whose HRSV is under 1 km (red stars), storms that have a HRSV over 1 km (black stars), and all storms are listed for each bin.

Storm Relative Helicity: 0-1 km SRH and ESRH

Interrogation of 0-1 km storm relative helicity (SRH), a measure of the potential for cyclonic updraft rotation in right-moving supercells (SPC 2016), was also performed in addition to effective SRH (ESRH). ESRH is calculated using thresholded CAPE and CIN values which are meant to confine the SRH layer to the part of the sounding where lifted parcels are buoyant (Thompson et al. 2007; SPC 2016). Across all storms, the association between mean HAE at the base-level scan and 0-1 km SRH is weak. The strongest correlations between mean HAE and 0-1 km SRH were in nontornadic storms with a HRSV greater than 1 km ($r = -0.255$).

Further analysis of all storms with HRSV greater than 1 km shows that HIGH 0-1 km SRH environments are associated with mean HAE of $\sim 53 \text{ km}^2$, whereas all other environments have a mean HAE of $\sim 101 \text{ km}^2$ ($p = 0.05$). In nontornadic storms with a mean HRSV below 1 km, LOW ESRH environments produce a mean HAE of $\sim 43 \text{ km}^2$ while HIGH ESRH environments produce a mean HAE of $\sim 119 \text{ km}^2$ ($p = 0.07$); additionally, HIGH environments produce a statistically significant difference in mean HAE when compared to all other environments (average HAE of $\sim 53 \text{ km}^2$; $p = 0.07$).

Even though variability in HAE was not well correlated with 0-1 km SRH, the strongest correlations were seen when looking at tornadic storms. Variability of tornadic storms with a HRSV greater than 1 km produce the strongest correlations of any data subsets ($r = 0.368$, respectively). Further analysis of all storms with a HRSV less than 1 km showed that HIGH ESRH environments have a mean variability of ~ 0.516 while all

other environments have a mean variability of ~ 0.592 , which is a significant difference ($p = 0.05$).

Hodograph Type

Hail production and variability has been shown to be affected by the hodograph shape in previous modeling studies (e.g., Adlerman and Droegemeier 2005; Van Den Broeke et al. 2010). Varying wind profiles have also produced differences in storm intensity and morphology in modeling studies (e.g., McCaul and Weisman 2001). Simulations in Van Den Broeke et al. (2010) showed that hail mixing ratio was higher in storms with full-circle hodographs, as areas near the updraft could contain many ice particles which could serve as hail embryos. Table 5.5 summarizes the categorization of hodograph types used for this analysis while Table 5.6 summarizes the sample sizes obtained for the different hodograph types.

Table 5.5: Name and description used when classifying hodograph types. A representative example of each hodograph type is also included.

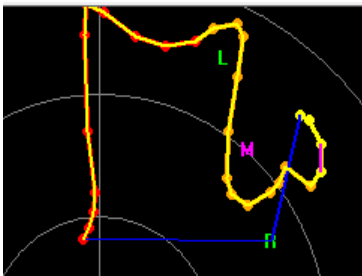
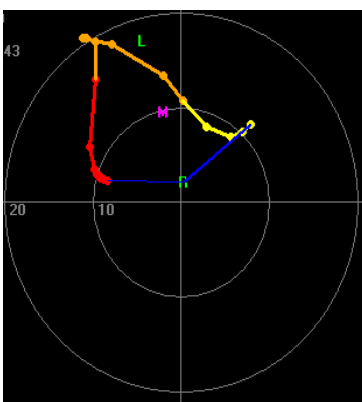
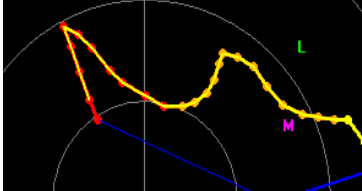
Classification	Description	Example
Segmented	Has well-defined segment(s) with cyclonic and anticyclonic curvature	
Curved	Dominated by cyclonic OR anticyclonic curvature through most of the 0-6 km depth	
Linear	Mostly straight-line; weak curvature through most of the 0-6 km depth	

Table 5.6: Summary of dominant hodograph type for six subsets of data. Sample size (n) and percentage of storms within that subset.

Height	Tornadic/Nontornadic	Dominant Hodograph Type	n (%)
Below 1 km	Nontornadic	Linear	9 (41%)
Above 1 km	Nontornadic	Curved	13 (48%)
Below 1 km	Tornadic	Curved	19 (43%)
Above 1 km	Tornadic	Segmented	19 (41%)
Below 1 km	All Storms	Curved	26 (39%)
Above 1 km	All Storms	Curved	24 (36%)

These overarching results were broken down into two bins differentiated by the mean value (Table 5.4) for both mean HAE and hail variability. Looking at tornadic environments with a HRSV under 1 km showed that 50% of these storms have either a curved or a segmented hodograph and a HAE below the mean value (n = 11 in both cases). In tornadic environments with a HRSV above 1 km, 10 storms (22%) have a segmented hodograph and a mean HAE below the 50th percentile, while 9 storms (20%) have a segmented hodograph and a mean HAE above the 50th percentile. There is no clear pattern of hodograph type in nontornadic environments with a HRSV below 1 km,

whereas nearly 41% ($n = 11$) of nontornadic environments with a HRSV above 1 km have a curved hodograph and a mean HAE above the 50th percentile.

Looking at hail variability, 25% ($n = 11$) of storms in tornadic environments with a HRSV < 1 km have variability values less than the 50th percentile and curved hodographs. Meanwhile, 24% ($n = 11$) of storms in these same environments and a HRSV above 1 km have straight hodographs and variability values greater than the 50th percentile. Analysis of storms in nontornadic environments, show that 26% ($n = 7$) of storms have a linear hodograph when the HRSV was greater than 1 km while 27% ($n = 6$) of storms have the same type of hodograph when the HRSV was less than 1 km; both of these produce hail variabilities greater than the 50th percentile. Further analysis shows that none of the hodograph types produce a significant difference in mean HAE or hail variability.

IV. Predictive Models for HAE and Hail Variability

A final step was to calculate predictive equations for both mean HAE and hail variability for different data subsets through multiple linear regression. Variables were included in the derivation of a predictive equation if the magnitude of the correlation coefficient between that variable and the subset of data was greater than 0.2. Since only a few variables had this strong of a relationship when looking at hail variability, the threshold was lowered to 0.1 for those predictive equations. Collinearity between the variables was checked using the Belsley condition index (Belsley et al. 2005); this greatly increases confidence in the value of the predictive equations as it allows for removal of

variables that are linearly dependent. Variables that have a condition index greater than 30 exhibit collinearity, and one of these variables would need to be removed from the analysis.

When looking at mean HAE, the following equation was developed for storms in tornadic environments with a HRSV above 1 km:

$$\begin{aligned} HAE (km^2) = & 3.07 \cdot 10^{-2}(a) - 2.41 \cdot 10^{-1}(b) + 3.97 \cdot 10^{-2}(c) \\ & - 1.96 \cdot 10^{-2}(d) + 4.64 \cdot 10^{-1}(e) - 9.93 \cdot 10^{-1}(f) - 6.46 \cdot 10^{-1}(g) \end{aligned} \quad (10)$$

where a is MUCAPE ($J kg^{-1}$), b is CIN ($J kg^{-1}$), c is LFC height (m), d is ambient $0^\circ C$ level (m), e is 1 km RH (%), f is 0-1 km shear (kt.), and g is ESHEAR (kt.). These variables were determined not to be collinear as the maximum condition index (MCI) was 21.6. This equation predicts 74.9% of the changes in mean HAE in tornadic storms with a HRSV > 1 km (Fig. 5.25). Meanwhile, 50.4% of the changes in mean HAE is predicted in tornadic storms with a mean HRSV < 1 km (MCI = 20.6) and approximately 44% of mean HAE is predicted in any tornadic storm (MCI = 22.9; Fig. 5.26) by the following equations, respectively:

$$\begin{aligned} HAE \text{ in tornadic storms } < 1 \text{ km } (km^2) = & 2.57 \cdot 10^{-1}(a) - 6.1 \cdot 10^{-3}(b) \\ & - 2.39(c) - 9.29 \cdot 10^{-2}(d) + 7.2 \cdot 10^{-1}(e) + 1.24(f) \end{aligned} \quad (11)$$

$$\begin{aligned} HAE \text{ in all tornadic storms } (km^2) = & 2.33 \cdot 10^{-1}(a) - 1.01 \cdot 10^{-2}(b) - 2.88(c) \\ & - 1.13 \cdot 10^{-1}(d) + 5.61 \cdot 10^{-1}(e) + 7.96 \cdot 10^{-1}(f) \\ & + 2.36 \cdot 10^{-1}(g) - 6 \cdot 10^{-3}(h) \end{aligned} \quad (12)$$

where a is CIN (J kg^{-1}), b is LFC height (m), c is LCL Temperature ($^{\circ}\text{C}$), d is 1 km RH (%), e is 1-3 km mean RH (%), f is ESHEAR (kt.), g is MUCAPE (J kg^{-1}), and h is ambient 0°C level (m). If the one extreme event (circled in red; Fig. 5.26) is removed from this last dataset, the predictability falls to 41.7%.

For comparison, HAE predictive equations were also derived for all supercells in tornadic environments, regardless of whether or not a tornado was produced. Predictability for mean HAE is slightly lower for all tornadic storms (~39%) and tornadic storms with a mean HRSV less than 1 km (~50%); meanwhile, predictability is substantially lower for tornadic storms greater than 1 km in height (~48% compared to ~75%). This underscores the importance of choosing tornadic supercells in similar work and increases the confidence that environmental variables may be able to differentiate tornadic from nontornadic storms, even in similar environments.

The predictability of HAE in tornadic storms less than 1 km in height is comparable to that predicted by the model of Van Den Broeke (2016; 51.2%). Although both models include LFC height and CIN, the previously developed model (Eq. 4) and the model developed in this study include different moisture parameters. Previously only 6-km RH was included while this study includes 1-km RH and the mean pressure weighted RH in the 1-3 km layer. Additional thermodynamic parameters (MUCAPE and LCL temperature), as well as ESHEAR, are also included in the predictive equation developed in this study. There may be a couple reasons for the small differences in predictability: the relatively small sample size used and the inclusion of both tornadic and nontornadic environments in the previous study.

Meanwhile, the following equation predicts 41.4% of the changes in mean HAE in storms in nontornadic environments with a HRSV ≥ 1 km (MCI = 19.8):

$$\begin{aligned} HAE (km^2) = & -3.12 \cdot 10^{-2}(a) - 1.93(b) + 3.65(c) \\ & + 4.55(d) + 1.94(e) - 5.83 \cdot 10^{-1}(f) - 4.54 \cdot 10^{-2}(g) \end{aligned} \quad (13)$$

where a is ambient 0°C height (m), b is 1-3 km mean RH (%), c is 3-6 km RH (%), d is 0-6 km shear, e is ESHEAR (kt.), and f and g are 0-1 and 0-3 km SRH ($\text{m}^2 \text{s}^{-2}$) respectively. Out of the three subsets of nontornadic storms, nontornadic storms with a mean HRSV greater than 1 km have the greatest predictability (Fig. 5.27). Looking at all storms, HAE is best predicted for storms greater than 1 km in height by:

$$\begin{aligned} HAE (km^2) = & 254.18 + 2.89 \cdot 10^{-2}(a) + 2.82 \cdot 10^{-2}(b) + 1.95 \cdot 10^{-2}(c) \\ & - 5.64 \cdot 10^{-2}(d) - 4.45 \cdot 10^{-1}(e) - 2.58 \cdot 10^{-1}(f) - 2.12(g) \end{aligned} \quad (14)$$

where a is MUCAPE (J kg^{-1}), b is CIN (J kg^{-1}), c is LFC height (m), d is 0°C height (m), e is 1 km RH (%), f is 1-3 km RH (%), and g is 0-1 km shear (MCI: 26.0), which explains 48.8% of the mean HAE.

Equations were also developed for the predictability of hail variability; overall, hail variability currently is not very predictable given the environmental variables analyzed. Hail variability was best predicted in nontornadic storms greater than 1 km in height where 37.1% of the variability is predicted (MCI: 12.5; Fig. 5.28):

$$\begin{aligned} c_v = & 1.0 \cdot 10^{-4}(a) + 1.33 \cdot 10^{-2}(b) + 3.2 \cdot 10^{-3}(c) \\ & - 1.99 \cdot 10^{-2}(d) + 9.0 \cdot 10^{-3}(e) + 3.0 \cdot 10^{-4}(f) \end{aligned} \quad (15)$$

where a is LFC height (m), b is LCL temperature ($^\circ\text{C}$), c is 3-9 km RH(%), d is 0-1 km shear (kt.), e is ESHEAR (kt.), and f is ESRH ($\text{m}^2 \text{s}^{-2}$). Predictability of hail variability in

tornadic storms (not shown) ranges from 10.7% (all tornadic storms) to 25.8% (tornadic storms with a HRSV greater than 1 km); additionally, hail variability in all storms was not predictable using environmental variables as predictability ranges from 1.9% to 12.1%.

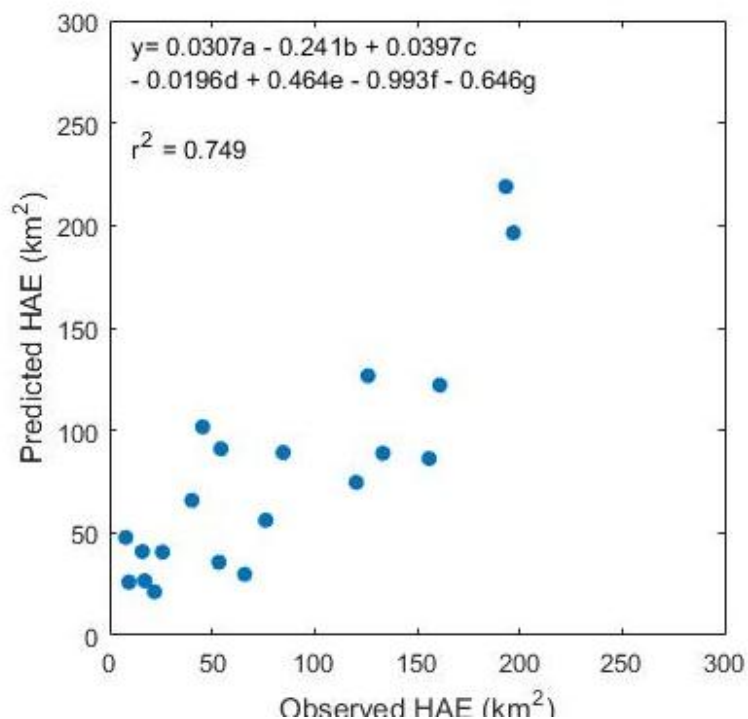


Fig. 5.25: Observed HAE (km²) vs. predicted HAE (km²) for storms in tornadic environments with a HRSV > 1 km. The equation used to obtain the predicted HAE (refer to text for variables corresponding to letters) and correlation coefficient (r^2) between datasets are given.

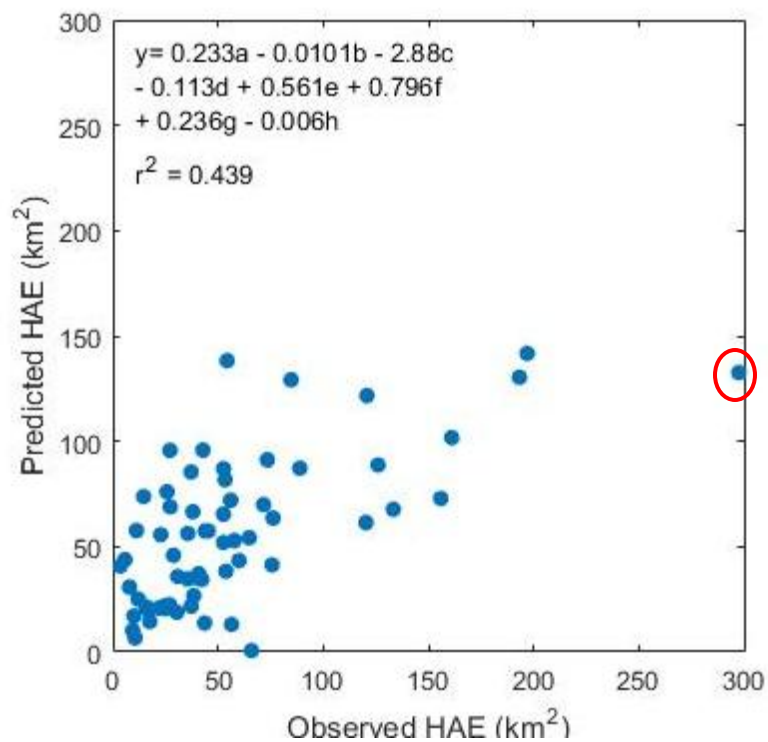


Fig. 5.26: Observed HAE (km^2) vs. predicted HAE (km^2) for all storms in tornadic environments. The equation used to obtain the predicted HAE (refer to text for variables corresponding to letters) and correlation coefficient (r^2) between datasets are given. The correlation coefficient (r^2) was 0.417 with the extreme event (circled in red) removed.

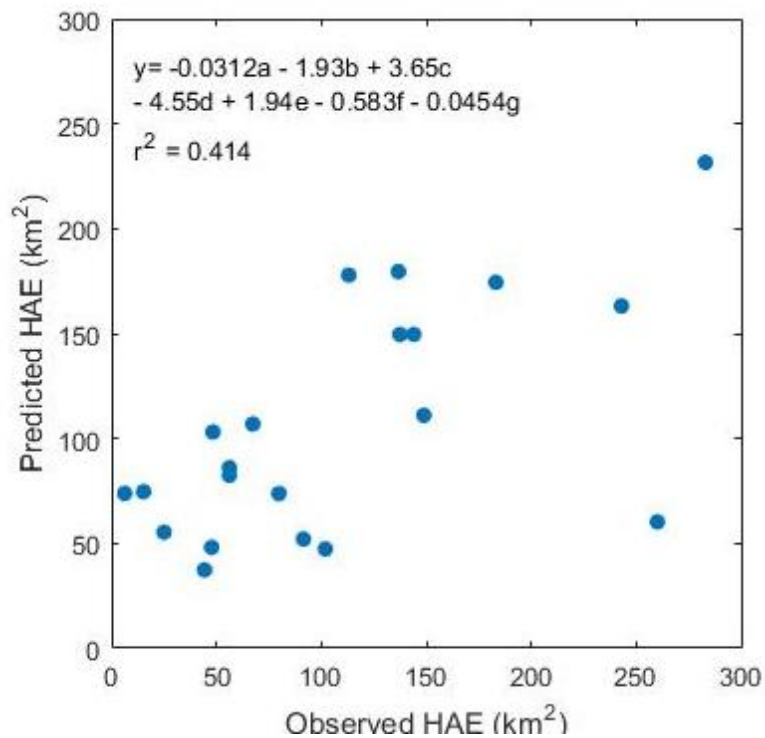


Fig. 5.27: Observed HAE (km²) vs. predicted HAE (km²) for storms in nontornadic environments with a HRSV > 1 km. The equation used to obtain the predicted HAE (refer to text for variables corresponding to letters) and correlation coefficient (r^2) between datasets are given.

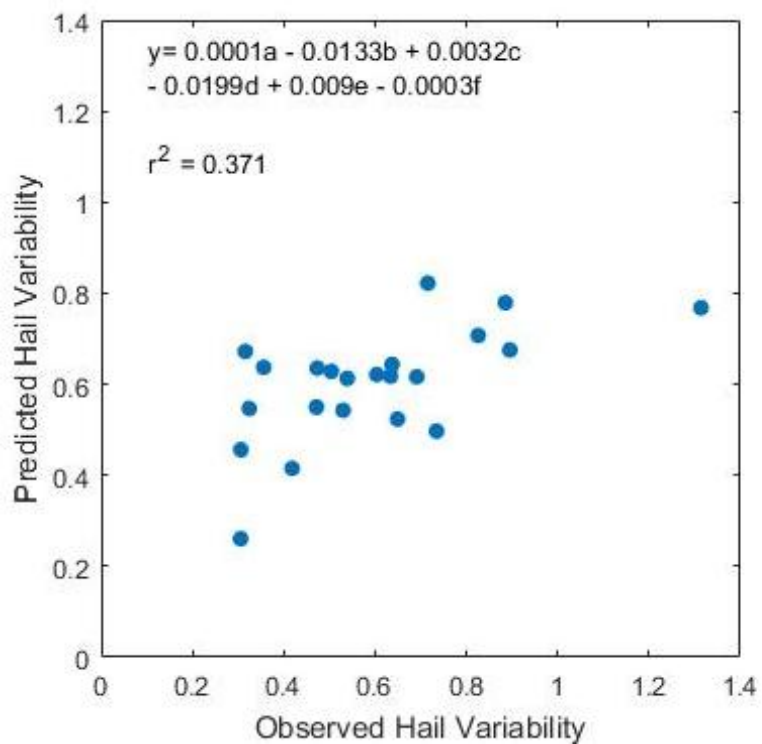


Fig. 5.28: Observed hail variability vs. predicted hail variability for storms in nontornadic environments with a HRSV > 1 km. The equation used to obtain the predicted hail variability (refer to text for variables corresponding to letters) and correlation coefficient (r^2) between datasets are given.

Chapter 6. Summary and Conclusions

As storm morphology and evolution can be impacted by the amount of HAE as well as the variability of HAE, it is important to understand how these might change as a function of environment. Using a dataset composed of 123 supercells within ~125 km of a WSR-88D across differing environments, significant relationships were determined between thermodynamic, moisture, and shear parameters and *hail areal extent* inferred at the base-scan level and between these same parameters and the *variability of hail extent* within supercell storms. This study shows how environmental variability affects the amount of hailfall and its temporal variability in supercell storms.

Overall, a combination of thermodynamic, shear, and moisture parameters were predictive of the mean HAE in tornadic and nontornadic storms, while shear parameters were strongly associated with hail variability in these storms. Predictive equations were developed through multiple linear regression for both mean HAE and HAE variability (Equations 10 - 15). These equations increased confidence that environmental variables may be able to differentiate tornadic from nontornadic storms, even in similar environments as predictability was substantially decreased with the inclusion of nontornadic supercells in tornadic environments.

Strong differences between environments were seen in mean HAE when examining LFC height, with an increase in LFC height associated with an increase in mean HAE. This variable is likely to be useful for looking at supercell variability between environments in the future. Height of the ambient 0°C level also emerged as differentiating mean HAE among the data subsets. When looking at mean hail variability

among storms, however, there was no one environmental variable that differentiated among the different environments for the subsets examined. Additionally, previous research showed that HAE variability was dependent on whether the storms were tornadic or nontornadic (e.g., Kumjian and Ryzhkov 2008; Van Den Broeke 2016). Results presented here show that HAE variability was not dependent on whether storms were tornadic or nontornadic; one caveat is that results presented here are not directly analogous to previous results, as the method of comparing hail variability is different between these studies.

Results support previous research (e.g., Rasmussen and Straka 1998; Gilmore et al. 2004; Van Den Broeke 2014) as an increase in MUCAPE was associated with an increase in the mean HAE of storms. Additionally, there were significant differences in HAE across MUCAPE environments for all storms, providing observational evidence that hail production increases with stronger updrafts. There is also evidence that an increase in low-level shear produces an increase in mean HAE, which supports previous modeling studies (e.g., Gilmore et al. 2004; Van Den Broeke et al. 2010). One possible explanation for this result is that ice particles from nearby storms could have been advected and lofted into the region of the analyzed storm. However, when examining low-level shear and hail variability, results seem to contradict previous modeling studies. Adlerman and Droegemeier (2005) implied that an increase in shear values should lead to a reduction in hail variability as the mesocyclone cycling process will slow down and terminate with an increase in shear. Van Den Broeke (2010), however, showed that with the inclusion of ice-microphysics, hail should become more variable with higher shear.

Even though mean HAE and hail variability can be correlated to individual environmental parameters, as shown, it is important to remember that there is strong interdependence among several of the parameters included in the analysis, as noted earlier (Table 4.2). Not only are several variables likely conveying similar information (e.g., 0-1- and 0-3-km SRH), but there might be many factors not captured by the environmental variables included in this study that affect storm-scale evolution and microphysical processes in supercell storms. It is hoped that the results of this study provide a foundation for the prediction of hailfall areal extent based on representative environmental conditions. Future work in this area may include adding to this dataset from after 2014 to continue trying to understand the microphysics of hail growth and hail variability more in depth, as well as breaking down the dataset to see if there are regional and seasonal differences in the response of hail areal extent to environmental variables, as different regions and seasons have different threshold values for several of the variables analyzed.

REFERENCES

- Adlerman, E.J., and K.K. Droegemeier, 2005: The dependence of numerically simulated cyclic mesocyclogenesis upon environmental vertical wind shear. *Mon. Wea. Rev.*, **133**, 3595-3623. doi: 10.1175/MWR3039.1.
- Auer, A.H., 1972: Distribution of graupel and hail with size. *Mon Wea Rev.*, **100**, 325-328. doi: 10.1175/1520-0493-100-05-0325.
- Balakrishnan, N. and D.S. Zrnić, 1990: Use of polarization to characterize precipitation and discriminate large hail. *J. Atmos. Sci.*, **47**, 1525-1540. doi: 10.1175/1520-0469(1990)047<1525:UOPTCP>2.0.CO;2.
- Beatty, K., E.N. Rasmussen, and J.M. Straka, 2008: The supercell spectrum. Part I: A review of research related to supercell precipitation morphology. *Electron. J. Severe Storms Meteor.*, **3** (4). [Available online at <http://www.ejssm.org/ojs/index.php/ejssm/article/view/44/46>.]
- Belsley, D.A., E. Kuh, and R.E. Welsh, 2005: *Regression Diagnostics: Identifying Influential Data and Sources of Collinearity*. John Wiley and Sons. 292 pp.
- Benjamin, S.G. and Coauthors, 2016: A North American hourly assimilation and model forecast cycle: The rapid refresh. *Mon. Wea. Rev.*, **144**, 1669-1694. doi: 10.1175/MWR-D-15-0242.1.
- Boustead, J.M., B.E. Mayes, W. Gargan, J.L. Leighton, G. Phillips, and P.N. Schumacher, 2013: Discriminating environmental conditions for significant warm sector and boundary tornadoes in parts of the Great Plains. *Wea. Forecasting*, **28**, 1498-1523. doi: 10.1175/WAF-D-12-00102.1.
- Brooks, H.E. and R.B. Wilhelmson, 1993: Hodograph curvature and updraft intensity in numerically modeled supercells. *J. Atmos. Sci.*, **50**, 1824-1833. doi: 10.1175/1520-0469(1993)050<1824:HCAUII>2.0.CO;2.
- , C.A. Doswell, and J. Cooper, 1994: On the environments of tornadic and nontornadic mesocyclones. *Wea. Forecasting*, **9**, 606-618. doi: 10.1175/1520-0434(1994)009<0606:OTEOTA>2.0.CO;2.
- Browning, K.A., 1965: The evolution of tornadic storms. *J. Atmos. Sci.*, **22**, 664-668. doi: 10.1175/1520-0469(1965)022<0664:TEOTS>2.0.CO;2.
- , and G.B. Foote, 1976: Airflow and hail growth in supercell storms and some implications for hail suppression. *Quart. J. Roy. Meteor.*, **102**, 499-533. doi: 10.1002/qj.49710243303.
- Bunkers, M.J., M.R. Hjelmfelt, and P.L. Smith, 2006: An observational examination of long-lived supercells. Part I: Characteristics, evolution, and demise. *Wea. Forecasting*, **21**, 673-688. doi: 10.1175/WAF949.1.
- Colby, F.P., 1984: Convective inhibition as a predictor of convection during AVE-SESAME II. *Mon. Wea. Rev.*, **112**, 2239-2252. doi: 10.1175/1520-0493(1984)112<2239:CIAAPO>2.0.CO;2.
- Davenport, C.E. and M.D. Parker, 2015: Impact of environmental heterogeneity on the dynamics of a dissipating supercell thunderstorm. *Mon. Wea. Rev.*, **143**, 4244-4277. doi: 10.1175/MWR-D-15-0072.1.
- Dennis, E.J., and M.R. Kumjian, 2014: The impact of hodograph shape on hail production in idealized supercell storms. *27th Conf. on Severe Local Storms*,

- Madison, WI, Amer. Meteor. Soc., P20. [Available online at https://ams.confex.com/ams/27SLS/webprogram/Manuscript/Paper255162/DennisKumjian_ExtendedAbstract_FINAL.pdf.]
- Doviak, R.J. and D.S. Zrnić, 1993: *Doppler Radar and Weather Observations*. Dover Publications, Inc. 562 pp.
- Evans, J.S. and C.A. Doswell, 2001: Examination of derecho environments using proximity soundings. *Wea. Forecasting*, **16**, 329-342. doi: 10.1175/1520-0434(2001)016<0329:EODEUP>2.0.CO;2.
- Everitt, B., 2002: *The Cambridge Dictionary of Statistics*. University Press. 410 pp.
- Finley, C.A., W.R., Cotton, and R.A. Pielke Sr., 2001: Numerical simulation of tornadogenesis in a high-precipitation supercell. Part I: Storm evolution and transition into a bow echo. *J. Atmos. Sci.*, **58**, 1597-1629. doi: 10.1175/1520-0469(2001)058<1597:NSOTIA>2.0.CO;2.
- Foote, G.B. and C.G. Wade, 1982: Case study of a hailstorm in Colorado. Part I: Radar echo structure and evolution. *J. Atmos. Sci.*, **39**, 2828-2846. doi: 10.1175/1520-0469(1982)039<2828:CSOAH1>2.0.CO;2.
- Gilmore, M.S. and L.J. Wicker, 1998: The influence of midtropospheric dryness on supercell morphology and evolution. *Mon. Wea. Rev.*, **126**, 943-958. doi: 10.1175/1520-0493(1998)126<0943:TIOMDO>2.0.CO;2.
- , J.M. Straka, and E.N. Rasmussen, 2004: Precipitation and evolution sensitivity in simulated deep convective storms: Comparisons between liquid-only and simple ice and liquid phase microphysics. *Mon. Wea. Rev.*, **132**, 1897-1916. doi: 10.1175/1520-0493(2004)132<1897:PAESIS>2.0.CO;2.
- Heinselman, P.L. and A.V. Ryzhkov, 2006: Validation of polarimetric hail detection. *Wea. Forecasting*, **21**, 839-850. doi: 10.1175/WAF956.1.
- Herzogh, P.H. and A.R. Jameson, 1992: Observing precipitation through dual-polarization radar measurements. *Bull. Amer. Meteor. Soc.*, **73**, 1365-1374. doi: 10.1175/1520-0477(1992)073<1365:OPTDPR>2.0.CO;2.
- Houston, A.L., R.L. Thompson, and R. Edwards, 2008: The optimal bulk wind differential depth and the utility of the upper-tropospheric storm-relative flow for forecasting supercells. *Wea. Forecasting.*, **23**, 825-837. doi: 10.1175/2008WAF2007007.1.
- Hubbert, J., V.N. Bringi, L.D. Carey, and S. Bolen, 1998: CSU-CHILL polarimetric radar measurements from a severe hail storm in eastern Colorado. *J. Appl. Meteor.*, **37**, 749-775. doi: 10.1175/1520-0450(1998)037<0749:CCPRMF>2.0.CO;2.
- James, R.P. and P.M. Markowski, 2010: A numerical investigation of the effects of dry air aloft on deep convection. *Mon. Wea. Rev.*, **138**, 140-161. doi:10.1175/2009MWR3018.1.
- Kaltenboeck, R., and A. Ryzhkov, 2013: Comparison of polarimetric signatures of hail at S and C bands for different hail sizes. *Atmos. Res.*, **123**, 323-336. doi: 10.1016/j.atmosres.2012.05.013.
- Karsten, C., 2010: National Bufkit Data Archive. Accessed 30 January 2015. [Available online at <http://www.meteor.iastate.edu/~ckarsten/bufkit/data/>.]

- Kennedy, P.C., S.A. Rutledge, B. Dolan, and E. Thaler, 2014: Observations of the 14 July 2011 Fort Collins hailstorm: Implications for WSR-88D-based hail detection and warnings. *Wea. Forecasting*, **29**, 623-638. doi: 10.1175/WAF-D-13-00075.1.
- Kirkpatrick, J.C., E.W. McCaul, and C. Cohen, 2007: The motion of simulated convective storms as a function of basic environmental parameters. *Mon. Wea. Rev.*, **135**, 3033-3051. doi: 10.1175/MWR3447.1.
- _____, _____, and _____, 2009: Variability of updraft and downdraft characteristics in a large parameter space study of convective storms. *Mon. Wea. Rev.*, **137**, 1550-1561. doi: 10.1175/2008MWR2703.1.
- _____, _____, and _____, 2011: Sensitivities of simulated convective storms to environmental CAPE. *Mon. Wea. Rev.*, **139**, 3514-3532. doi: 10.1175/2011MWR3631.1.
- Kumjian, M.R., and A.V. Ryzhkov, 2008: Polarimetric signatures in supercell thunderstorms. *J. Appl. Meteor. Climatol.*, **47**, 1940-1961. doi: 10.1175/2007JAMC1874.1.
- _____, 2011: Precipitation properties of supercell hook echoes. *Electron. J. Severe Storms Meteor.*, **6** (5). [Available online at <http://www.ejssm.org/ojs/index.php/ejssm/article/view/93>.]
- Lemon, L.R., 1977: New severe thunderstorm radar identification techniques and warning criteria: A preliminary report. NOAA Tech. Memo. NWS NSSFC-1, Kansas City, National Severe Storms Forecast Center, 60 pp.
- Lin, Y.J., and P.T. Chang, 1977: Some effects of the shearing and veering environmental wind on the internal dynamics and structure of a rotating supercell thunderstorm. *Mon. Wea. Rev.*, **105**, 987-997. doi: 10.1175/1520-0493(1977)105<0987:SEOTSA>2.0.CO;2.
- Liu, H. and V. Chandrasekar, 2000: Classification of hydrometeors based on polarimetric radar measurements: Development of fuzzy logic and neuro-fuzzy systems, and in situ verification. *J. Atmos. Oceanic Technol.*, **17**, 140-164. doi: 10.1175/1520-0426(2000)017<0140:COHBOP>2.0.CO;2.
- Markowski, P.M., J.M. Straka, E.N. Rasmussen, and D.O. Blanchard, 1998: Variability of storm relative helicity during VORTEX. *Mon. Wea. Rev.*, **126**, 2959-2971.
- McCaul, E.W. and M.L. Weisman, 2001: The sensitivity of simulated supercell structure and intensity to variations in the shapes of environmental buoyancy and shear profiles. *Mon. Wea. Rev.*, **129**, 664-687. doi: 10.1175/1520-0493(2001)129<0664:TSOSSS>2.0.CO;2.
- Moller, A.R., C.A. Doswell, M.P. Foster, and G.R. Woodall, 1994: The operational recognition of supercell thunderstorm environments and storm structures. *Wea. Forecasting*, **9**, 327-347. doi: 10.1175/1520-0434(1994)009<0327:TOROST>2.0.CO;2.
- Naylor, J., and M.S. Gilmore, 2014: Vorticity evolution leading to tornadogenesis and tornadogenesis failure in simulated supercells. *J. Atmos. Sci.*, **71**, 1201-1217. doi:10.1175/JAS-D-13-0219.1.

- National Oceanic and Atmospheric Administration (NOAA), 2014a: NEXRAD Data Archive, Inventory and Access. Accessed 31 October 2014. [Available online at <https://www.ncdc.noaa.gov/nexradinv/>.]
- National Oceanic and Atmospheric Administration (NOAA), 2014b: Storm Events Database. Accessed 2 October 2014. [Available online at <https://www.ncdc.noaa.gov/stormevents/>.]
- Park, H., A.V. Ryzhkov, D.S. Zrnić, and K.-E. Kim, 2009: The hydrometeor classification algorithm for the polarimetric WSR-88D: Description and application to an MCS. *Wea. Forecasting*, **24**, 730-748. doi: 10.1175/2008WAF2222205.1.
- Parker, M.D., 2014: Composite VORTEX2 supercell environments from near-storm soundings. *Mon. Wea. Rev.*, **142**, 508-529. doi: 10.1175/MWR-D-13-00167.1.
- Rasmussen, E.N., and D.O. Blanchard, 1998: A baseline climatology of sounding-derived supercell and tornado forecast parameters. *Wea. Forecasting*, **13**, 1148-1164. doi: 10.1175/1520-0434(1998)013<1148:ABCOSD>2.0.CO;2.
- , and J.M. Straka, 1998: Variations in supercell morphology. Part I: Observations of the role of upper-level storm-relative flow. *Mon. Wea. Rev.*, **126**, 2406-2421. doi: 10.1175/1520-0493(1998)126<2406:VISMPI>2.0.CO;2.
- , 2003: Refined supercell and tornado forecast parameters. *Wea. Forecasting*, **18**, 530-535. doi: 10.1175/1520-0434(2003)18<530:RSATFP>2.0.CO;2.
- Rasmussen, R.M., V. Levizzani, and H.R. Pruppacher, 1984a: A wind tunnel and theoretical study of the melting behavior of atmospheric ice particles. II: A theoretical study for frozen drops of radius < 500 μm . *J. Atmos. Sci.* **41**, 374-380. doi: 10.1175/1520-0469(1984)041<0374:AWTATS>2.0.CO;2.
- , —————, and —————, 1984b: A wind tunnel and theoretical study of the melting behavior of atmospheric ice particles. III: A theoretical study for frozen drops of radius > 500 μm . *J. Atmos. Sci.* **41**, 381-388. doi: 10.1175/1520-0469(1984)041<0381:AWTATS>2.0.CO;2.
- , and A.J. Heymsfield, 1987: Melting and shedding of graupel and hail. Part II: Sensitivity study. *J. Atmos. Sci.*, **44**, 2764-2782. doi: 10.1175/1520-0469(1987)044<2764:MASOGA>2.0.CO;2.
- Rinehart, R.E., 1991: *Radar for Meteorologists, or You too can be a Radar Meteorologist*. Department of Atmospheric Sciences, University of North Dakota. 334 pp.
- Rogers, R.R. and M.K. Yau, 1989: *A Short Course in Cloud Physics*. Butterworth Heinemann. 290 pp.
- Shabbot, C.J., and P.M. Markowski, 2006: Surface in situ observations within the outflow of forward-flank downdrafts of supercell thunderstorms. *Mon. Wea. Rev.*, **134**, 1422-1441. doi: 10.1175/MWR3131.1.
- Srivastava, R.C., 1987: A model of intense downdrafts driven by the melting and evaporation of precipitation. *J. Atmos. Sci.*, **44**, 1752-1773. doi: 10.1175/1520-0469(1987)044<1752:AMOIDD>2.0.CO;2.

- Storm Prediction Center (SPC), 2016: Explanation of SPC severe weather parameters. Accessed 25 October 2016. [Available online at <http://www.spc.noaa.gov/sfctest/help/sfcoa.html>.]
- Straka, J.M., D.S. Zrnić, and A.V. Ryzhkov, 2000: Bulk hydrometeor classification and quantification using polarimetric radar data: Synthesis of relations. *J. Appl. Meteor.*, **39**, 1341-1372. doi: 10.1175/1520-0450(2000)039<1341:BHCAQU>2.0.CO;2.
- Stumpf, G.J, A.Witt, E.D. Mitchell, P.L. Spencer, J.T. Johnson, M.D. Eilts, K.W. Thomas, and D.W. Burgess, 1998: The National Severe Storms Laboratory mesocyclone detection algorithm for the WSR-88D. *Wea. Forecasting*, **13**, 304-326. doi: 10.1175/1520-0434(1998)013<0304:TNSSLM>2.0.CO;2.
- Thompson, R.L., R. Edwards, J.A. Hart, K.L. Elmore, and P. Markowski, 2003: Close proximity soundings within supercell environments obtained from the rapid update cycle. *Wea. Forecasting*, **18**, 1243-1261. doi: 10.1175/1520-0434(2003)018<1243:CPSWSE>2.0.CO;2.
- , C.M. Mead, and R. Edwards, 2007: Effective storm-relative helicity and bulk shear in supercell thunderstorm environments. *Wea. Forecasting*, **22**, 102-115. doi: 10.1175/WAF969.1.
- , B.T. Smith, J.S. Grams, A.R. Dean, C. Bowles, 2012: Convective modes for significant severe thunderstorms in the contiguous United States. Part II: Supercell and QLCS tornado environments. *Wea. Forecasting*, **27**, 1136-1154. doi: 10.1175/WAF-D-11-00116.1.
- Van Den Broeke, M.S., J.M. Straka, and E.N. Rasmussen, 2008: Polarimetric radar observations at low levels during tornado life cycles in a small sample of classic southern plains supercells. *J. Appl. Meteor. Climatol.*, **47**, 1232-1247. doi: 10.1175/2007JAMC1714.1.
- , —————, and —————, 2010: Mesocyclone and RFD evolution in simulated supercell storms with varying wind profiles. *25th Conf. on Severe Local Storms*, Denver, CO, Amer. Meteor. Soc., 8A.6. [Available online at <https://ams.confex.com/ams/pdfpapers/175852.pdf>.]
- , 2014: Effects of mid- and upper-level drying on microphysics of simulated supercell storms. *Electron. J. Severe Storms Meteor.*, **9** (3). [Available online at <http://www.ejssm.org/ojs/index.php/ejssm/article/view/134/99>.]
- , 2016: Polarimetric variability of classic supercell storms as a function of environment. *J. Appl. Meteor. Climatol.*, **55**, 1907-1925. doi: 10.1175/JAMC-D-15-0346.1.
- van den Heever, S.C. and W.R. Cotton, 2004: The impact of hail size on simulated supercell storms. *J. Atmos. Sci.*, **61**, 1596-1609. doi: 10.1175/1520-0469(2004)061<1596:TIOHSO>2.0.CO;2.
- Warning Decision Training Division (WDTD), 2013: Dual-polarization radar training for NWS partners. Accessed 18 October 2016. [Available online at <http://www.wdtb.noaa.gov/courses/dualpol/Outreach/>.]

- Weisman, M.L. and J.B. Klemp, 1982: The dependence of numerically simulated convective storms on vertical wind shear and buoyancy. *Mon. Wea. Rev.*, **110**, 504-520. doi: 10.1175/1520-0493(1982)110<0504:TDONSC>2.0.CO;2.
- and —————, 1984: The structure and classification of numerically simulated convective storms in directionally varying wind shears. *Mon. Wea. Rev.*, **112**, 2479-2498. doi: 10.1175/1520-0493(1984)112<2479:TSACON>2.0.CO;2.
- Wilks, D.S., 2006: *Statistical Methods in the Atmospheric Sciences*. Academic Press. 627 pp.
- Zrnić, D.S. and A.V. Ryzhkov, 1999: Polarimetry for weather surveillance radars. *Bull. Amer. Meteor. Soc.*, **80**, 389-406.